Neuron

Article

Proneural genes define ground-state rules to regulate neurogenic patterning and cortical folding

Graphical abstract

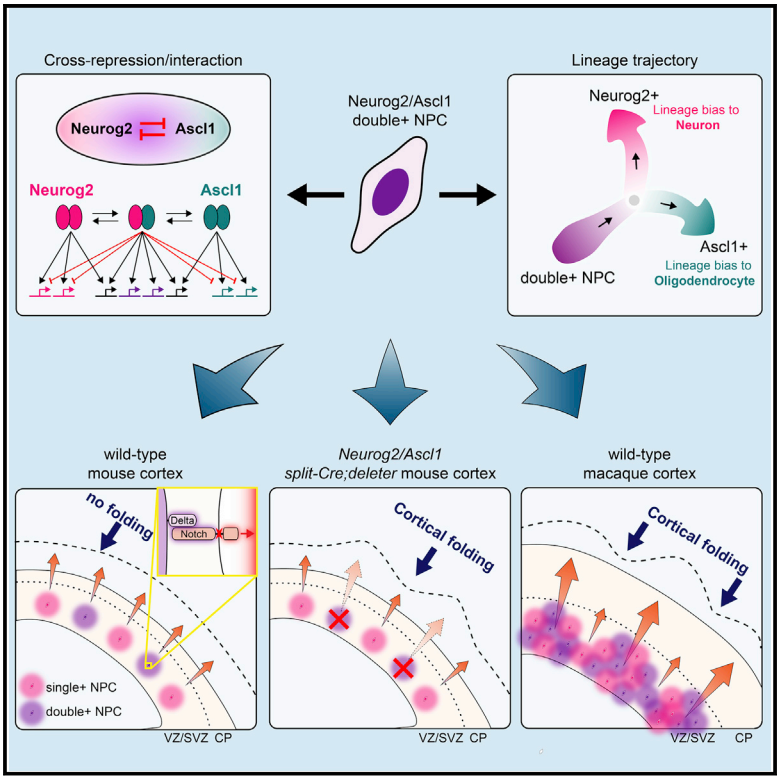

Highlights

- *Neurog2* and *Ascl1* proneural gene expression defines four transitional NPC states
- Neurog2-Ascl1 cross-repress to block lineage bias of double^{+} NPCs at hierarchy apex
- Double^{+} NPCs direct uniform neurogenesis via Notch to sustain murine lissencephaly
- *NEUROG2*, *ASCL1*, and *HES1* expression is modular in gyrencephalic macaque cortices

Authors

Sisu Han, Satoshi Okawa, Grey Atteridge Wilkinson, ..., Jeff Biernaskie, Antonio del Sol, Carol Schuurmans

Correspondence

cschuurm@sri.utoronto.ca

In brief

Emergence of a gyrencephalic cortex is associated with a break in neurogenic continuity across the cortical germinal zone. Han et al. identify a pool of unbiased neural progenitor cells at a lineage bifurcation point that co-express *Neurog2* and *Ascl1* and produce Notch ligands to control neurogenic periodicity and cortical folding.

Han et al., 2021, Neuron *109*, 1–17
September 15, 2021
https://doi.org/10.1016/j.neuron.2021.07.007

CellPress

Neuron

CellPress

Article

Proneural genes define ground-state rules to regulate neurogenic patterning and cortical folding

Sisu Han,[1,2] Satoshi Okawa,[3,4,20] Grey Atteridge Wilkinson,[5,20] Hussein Ghazale,[1,2] Lata Adnani,[1,5] Rajiv Dixit,[1,2] Ligia Tavares,[6] Imrul Faisal,[1,2] Matthew J. Brooks,[7] Veronique Cortay,[8] Dawn Zinyk,[1] Adam Sivitilli,[2,9] Saiqun Li,[5,17] Faizan Malik,[10] Yaroslav Ilnytskyy,[11] Vladimir Espinosa Angarica,[3] Jinghua Gao,[1,2] Vorapin Chinchalongporn,[1,2] Ana-Maria Oproescu,[1,12] Lakshmy Vasan,[1,12] Yacine Touahri,[1,2] Luke Ajay David,[1,12] Eko Raharjo,[13] Jung-Woong Kim,[7,18] Wei Wu,[14,19] Waleed Rahmani,[13] Jennifer Ai-wen Chan,[14] Igor Kovalchuk,[11] Liliana Attisano,[2,9] Deborah Kurrasch,[10] Colette Dehay,[8] Anand Swaroop,[7] Diogo S. Castro,[6] Jeff Biernaskie,[13] Antonio del Sol,[3,15,16] and Carol Schuurmans[1,2,5,12,21,*]

[1]Sunnybrook Research Institute, 2075 Bayview Ave, Toronto, ON M4N 3M5, Canada
[2]Department of Biochemistry, University of Toronto, Toronto, ON M5S 1A8, Canada
[3]Computational Biology Group, Luxembourg Centre for Systems Biomedicine, University of Luxembourg, 4362 Esch-sur-Alzette, Luxembourg
[4]Integrated BioBank of Luxembourg, 3555, 3531 Dudelange, Luxembourg
[5]Department of Biochemistry and Molecular Biology, ACHRI, HBI, University of Calgary, Calgary, AB T2N 4N1, Canada
[6]i3S-Instituto de Investigação e Inovação em Saúde, Universidade do Porto, Rua Alfredo Allen, 208, 4200-135 Porto, Portugal
[7]Neurobiology-Neurodegeneration & Repair Laboratory, National Eye Institute, National Institutes of Health, Bethesda, MD 20892-1204, USA
[8]Université Claude Bernard Lyon 1, Inserm, Stem Cell and Brain Research Institute U1208, 69500 Bron, France
[9]Donnelly Centre, University of Toronto, Toronto, ON M5S 3E1, Canada
[10]Department of Medical Genetics, ACHRI, HBI, University of Calgary, Calgary, AB T2N 4N1, Canada
[11]Department of Biological Sciences, University of Lethbridge, Lethbridge, AB T1K 3M4, Canada
[12]Department of Laboratory Medicine and Pathobiology, University of Toronto, Toronto, ON M5S 1A8, Canada
[13]Department of Comparative Biology and Experimental Medicine, HBI, ACHRI, University of Calgary, Calgary, AB T2N 4N1, Canada
[14]Department of Pathology and Laboratory Medicine, Charbonneau Cancer Institute, HBI, University of Calgary, Calgary, AB T2N 4Z6, Canada
[15]CIC bioGUNE, Bizkaia Technology Park, 48160 Derio, Spain
[16]IKERBASQUE, Basque Foundation for Science, Bilbao 48013, Spain
[17]Present address: State Key Laboratory of Ophthalmology, Zhongshan Ophthalmic Center, SunYat-sen University, Guangzhou 510060, China
[18]Present address: Department of Life Science, Chung-Ang University, 84 Heukseok-ro, Dongjak-gu, Seoul 06974, Korea
[19]Present address: Helen Diller Family Comprehensive Cancer Center, University of California San Francisco, San Francisco, CA, USA
[20]These authors contributed equally
[21]Lead contact
*Correspondence: cschuurm@sri.utoronto.ca
https://doi.org/10.1016/j.neuron.2021.07.007

SUMMARY

Asymmetric neuronal expansion is thought to drive evolutionary transitions between lissencephalic and gyrencephalic cerebral cortices. We report that *Neurog2* and *Ascl1* proneural genes together sustain neurogenic continuity and lissencephaly in rodent cortices. Using transgenic reporter mice and human cerebral organoids, we found that *Neurog2* and *Ascl1* expression defines a continuum of four lineage-biased neural progenitor cell (NPC) pools. Double$^+$ NPCs, at the hierarchical apex, are least lineage restricted due to Neurog2-Ascl1 cross-repression and display unique features of multipotency (more open chromatin, complex gene regulatory network, G_2 pausing). Strikingly, selectively eliminating double$^+$ NPCs by crossing *Neurog2-Ascl1* split-Cre mice with diphtheria toxin-dependent "deleter" strains locally disrupts Notch signaling, perturbs neurogenic symmetry, and triggers cortical folding. In support of our discovery that double$^+$ NPCs are Notch-ligand-expressing "niche" cells that control neurogenic periodicity and cortical folding, *NEUROG2*, *ASCL1*, and *HES1* transcript distribution is modular (adjacent high/low zones) in gyrencephalic macaque cortices, prefiguring future folds.

Please cite this article in press as: Han et al., Proneural genes define ground-state rules to regulate neurogenic patterning and cortical folding, Neuron (2021), https://doi.org/10.1016/j.neuron.2021.07.007

INTRODUCTION

The cerebral cortex has transitioned during evolution between smooth, lissencephalic forms in smaller mammals to highly folded, gyrencephalic structures in primates and larger mammals (Lewitus et al., 2014). Despite this phenotypic diversity, the underlying genetic programs that guide cortical development are conserved (Kriegstein et al., 2006), raising the question as to how built-in constraints have been modified to allow new cortical patterns to emerge. The blueprints for lissencephalic and gyrencephalic cortices are being deciphered, revealing a diversification of the central "building blocks"—the multipotent neural stem (NSC) and progenitor (NPCs, hereafter used collectively) cells that give rise to cortical neurons and glia. Apical NPCs, including apical radial glia (aRG), are more similar across species than basal NPCs, which show greater species divergence. In smooth cortices, basal NPCs include intermediate progenitor cells (IPCs), which have a limited proliferative capacity (Miyata et al., 2004), while in folded cortices, basal NPCs have expanded to form an outer subventricular zone (oSVZ) of IPCs and basal radial glia (bRG) (Reillo et al., 2011). IPCs and bRG self-amplify in macaque (Betizeau et al., 2013) and ferret (Martínez-Martinez et al., 2016), leading to an expansion of upper-layer neurons (layers 2/3), which become folded along with inner neuronal layers (layers 5/6).

There are local differences in cortical NPC proliferation in ferret, cat, and human cortices, with several-fold variations in mitotic density across the ferret germinal zone (Reillo et al., 2011). Moreover, when focal increases in proliferation are induced experimentally in mice, cortical folding ensues (Rash et al., 2013; Stahl et al., 2013). However, NPC expansion alone does not explain why primary gyri (outward folds) and sulci (inward fissures), which form in regions of high and low neurogenesis, respectively, develop in stereotyped positions (Reillo et al., 2011). Transcriptomic analyses of NPCs isolated from ferret gyri and sulci revealed that a genetic protomap pre-figures sites of cortical folding (de Juan Romero et al., 2015). This protomap, which does not exist in mouse, includes genes that control neurogenesis, suggesting that regional differences in NPC differentiation may spatially define where folds form (de Juan Romero et al., 2015).

Proneural basic-helix-loop-helix (bHLH) transcription factors (TFs) are the main drivers of NPC differentiation (Oproescu et al., 2021). *Neurog1* and *Neurog2* specify a glutamatergic neuronal fate in cortical NPCs, with *Neurog2* the dominant factor (Han et al., 2018), whereas *Ascl1* function in cortical NPCs is poorly understood. Here, we found that *Neurog2* and *Ascl1* expression defines four distinct NPC pools: proneural negative (pro$^-$) and pro$^+$ (Ascl1$^+$, Neurog2$^+$, double$^+$), each with unique lineage biases, transcriptomes, epigenomes, and gene regulatory networks (GRNs). Strikingly, when double$^+$ NPCs are deleted, the regularity of Notch signaling is disrupted and the rodent cortex forms folds. Intriguingly, while *Neurog2*, *Ascl1*, and *Hes1* expression is continuous in the murine cortex, it is modular (high/low zones) in the folded macaque cortex, supporting the idea that the differential regulation of Notch signaling by proneural genes controls neurogenic patterning and can drive cortical folding when discontinuous.

RESULTS

Neurog2 and *Ascl1* define four NPC pools in gyrencephalic and lissencephalic cortices

Lissencephalic cortices undergo uniform neurogenesis, while folding is associated with asymmetric neuronal expansion (Lewitus et al., 2014). We asked how *Neurog2*, the main cortical neuronal determinant (Han et al., 2018), and *Ascl1*, a proneural gene with poorly understood cortical functions, act together to support a lissencephalic pattern of neurogenesis in mice. At embryonic day 12.5 (E12.5), when neurogenesis begins, most DAPI$^+$ NPCs in the cortical ventricular zone (VZ) were pro$^-$ (78.6%), while pro$^+$ NPCs included Neurog2$^+$ (15.1%), Ascl1$^+$ (2.9%), and double$^+$ (3.4%) cells (Figure 1A). These distinct NPC pools persisted from E12.5 to E16.5, with the proportion of double$^+$ NPCs relatively stable, whereas Neurog2$^+$ ($p < 0.01$) and Ascl1$^+$ ($p < 0.01$) NPC numbers gradually increased (Figures 1A and S1A).

Using RNAscope, we identified the same pro$^-$, *NEUROG2*$^+$, *ASCL1*$^+$, and double$^+$ NPCs in E70 macaque cortices and 3-month-old human cerebral organoids (3-mo COs) (Figures 1B and 1C). Notably, the overall proportion of double$^+$ NPCs was higher than in mice, ranging from 25% in the macaque VZ/inner SVZ, where *PAX6*$^+$ aRG reside, 38% in the macaque oSVZ, containing *PAX6*$^+$*HOPX*$^+$ bRG, and 40.4% in 3-mo CO rosettes (Figures 1B, 1C, and S1B–S1D). We further mined single-cell RNA sequencing (scRNA-seq) data from 3-mo COs, identifying 20 clusters, including NPCs (aRG, bRG, IPCs) and various neuronal subtypes (Figure 1D) (Sivitilli et al., 2020). *NEUROG2* and *ASCL1* were expressed singly in aRG, bRG, IPCs, and some neurons, each with distinct patterns, while double$^+$ cells were almost exclusively NPCs (Figures 1D and 1E). Strikingly, in annotated scRNA-seq data from human fetal cortices (Zhong et al., 2018), of the 290 NPCs sequenced between gestational week 08 (GW08) and GW26, the majority (54.8%) were double$^+$ (Figure 1F).

We thus identified pro$^-$, Neurog2$^+$, Ascl1$^+$, and double$^+$ cortical NPCs in lissencephalic and gyrencephalic cortices and found an overall higher proportion of double$^+$ NPCs in human and non-human primates (NHPs).

Neurog2 and Ascl1 single$^+$ NPCs are more lineage biased than double$^+$ NPCs

To identify and interrogate double$^+$ NPC function, we generated *Neurog2*^{mCherryKI} knockin (KI) mice (Figures S1E–S1G) and created double KIs with *Ascl1*^{GFPKI} transgenics (Leung et al., 2007) (Figure 1G). We confirmed that mCherry labeled Neurog2$^+$ NPCs (90.3%) and GFP marked Ascl1$^+$ NPCs (86.1%), while both reporters also labeled preplate neurons, acting as short-term lineage tracers (Figures S1H and S1I). To assess cell fate bias *in vitro*, we isolated pro$^-$ (no reporter), Neurog2$^+$ (mCherry$^+$), Ascl1$^+$ (GFP$^+$), and double$^+$ (mCherry$^+$GFP$^+$) NPCs from E12.5 double KI cortices by fluorescence-activated cell sorting (FACS) and further selected for CD15 to enrich for NPCs over neurons (Ballas et al., 2005) (Figure 1H). By qPCR, we confirmed that CD15 marked part of a larger pool of CD133$^+$ NPCs, enriching for aRG over IPCs (Figures S1J–S1O) and that *Neurog2* and *Ascl1* were appropriately enriched in the sorted NPC pools (Figure S1P).

Using directed differentiation, E12.5 Neurog2$^+$ NPCs gave rise to more β3-tubulin$^+$ neurons than pro$^-$ NPCs, which we set as

Please cite this article in press as: Han et al., Proneural genes define ground-state rules to regulate neurogenic patterning and cortical folding, Neuron (2021), https://doi.org/10.1016/j.neuron.2021.07.007

CellPress

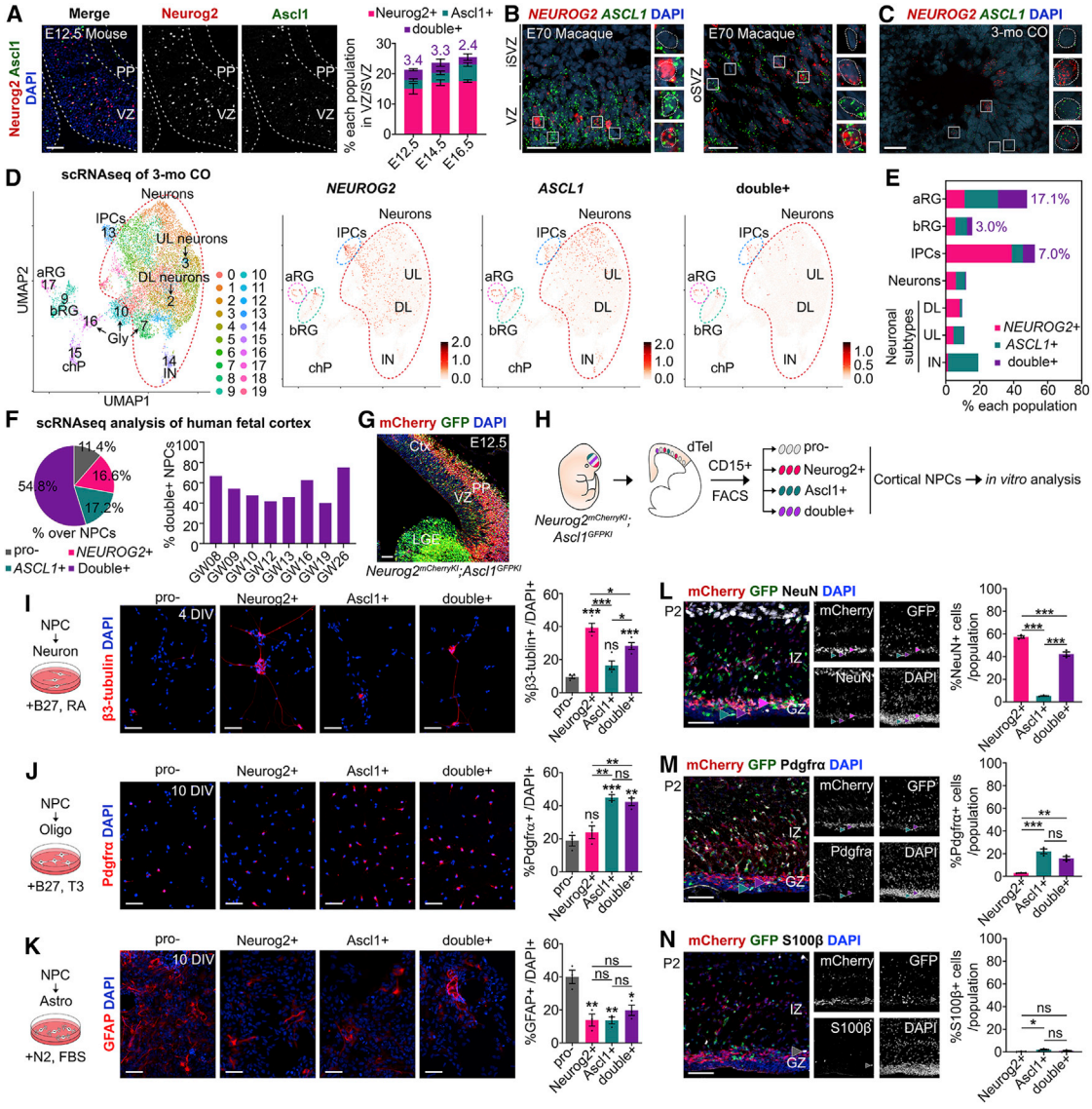

Figure 1. Neurog2 and Ascl1 expression defines four cortical NPC pools with distinct lineage biases

(A) Expression and quantification of DAPI$^+$ NPCs expressing Neurog2 and Ascl1 (N = 3/stage) in E12.5 mouse cortex.

(B and C) *NEUROG2* and *ASCL1* mRNA distribution in E70 macaque cortex (B) and 3-mo CO (C), with 2.5× magnified views.

(D and E) UMAP plot of scRNA-seq data from 3-mo COs, showing *NEUROG2*, *ASCL1*, and double$^+$ cells (D) and proportions of expressing cell types (N = 6 COs, 3 batches) (E).

(F) Quantification of *NEUROG2*$^+$, *ASCL1*$^+$, and double$^+$ cells in scRNA-seq data from human fetal cortices from GW08 to GW28.

(G) mCherry and GFP expression in E12.5 double KI.

(H) FACS protocol for CD15$^+$ cortical NPCs.

(I–K) Differentiation of E12.5 CD15$^+$ NPCs into β3-tubulin$^+$ neurons counted after 4 DIV (N = 4) (I), Pdgfrα$^+$ oligodendrocytes after 10 DIV (N = 3) (J), and GFAP$^+$ astrocytes after 10 DIV (N = 3) (K).

(L–N) Co-immunolabeling of mCherry$^+$ and/or GFP$^+$ cells in P2 double KI cortices with NeuN (L), Pdgfrα (M), and S100β (N) (N = 3 for all).

Data are represented as mean ± SEM. Two-way ANOVA and Tukey's post-hoc tests were used in (A). One-way ANOVA and Tukey's post-hoc tests were used in (I)–(N). p-values: ns - not significant, <0.05 *, <0.01 **, <0.001 ***. Scale bars in (A), (G), and (I)–(N), 50 μm; (B) and (C), 25 μm. aRG, apical radial glia; bRG, basal radial glia; chP, choroid plexus; Ctx, cortex; CO, cerebral organoid; DL, deep layer; Gly, high glycolytic cells; GW, gestational week; IN, interneuron; IPC, intermediate progenitor cell; iSVZ, inner subventricular zone; IZ, intermediate zone; LGE; lateral ganglionic eminence; oSVZ, outer subventricular zone; PP, preplate; UL, upper layer; VZ, ventricular zone.

See also Figure S1.

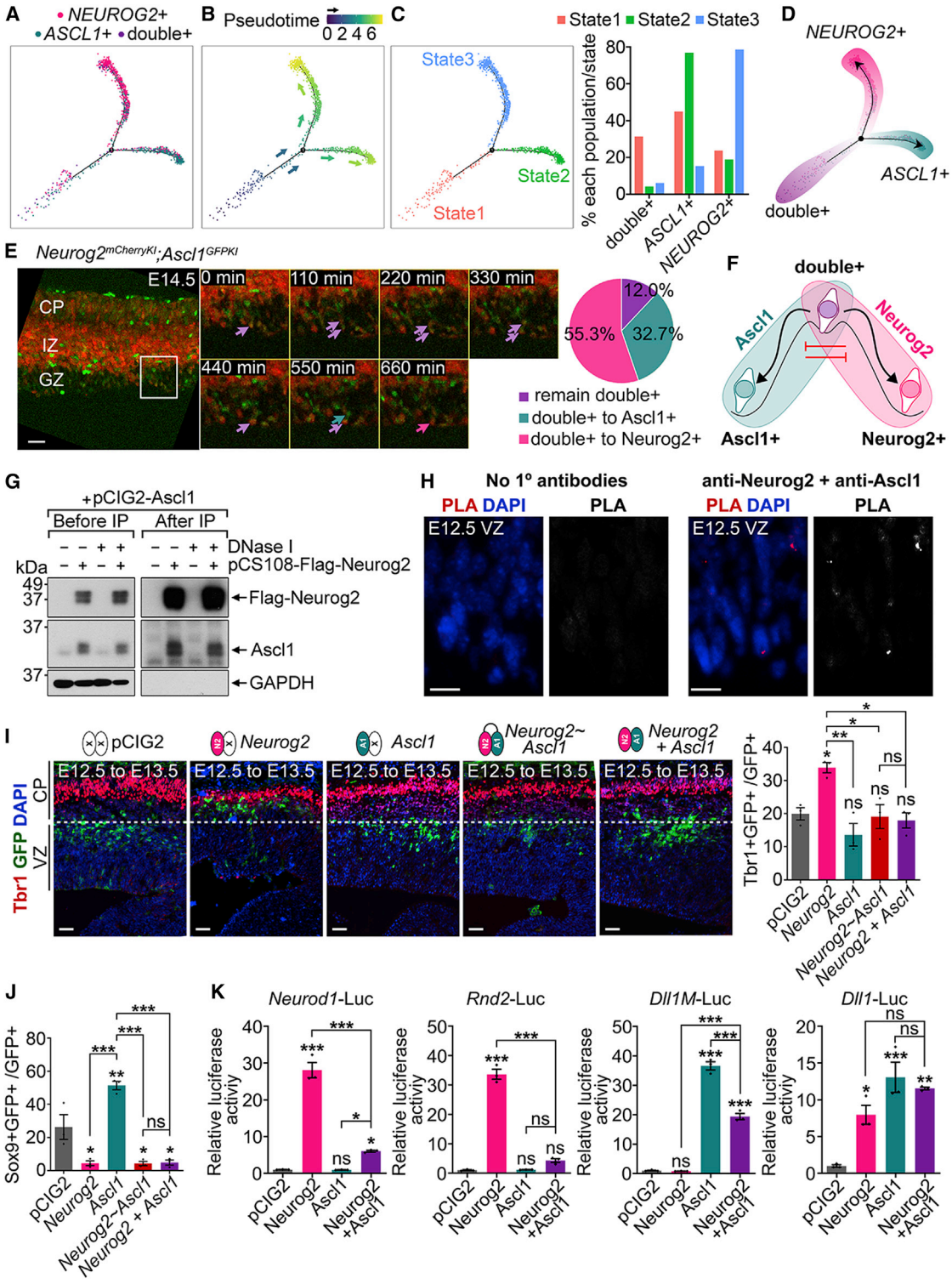

Figure 2. Double$^+$ NPCs mark a lineage bifurcation point and are maintained in multipotency via Neurog2-Ascl1 cross-repression

(A–D) Monocle3 lineage trajectory analysis of *NEUROG2*$^+$, *ASCL1*$^+$, and double$^+$ cells in 3-mo CO scRNA-seq data (A), showing a pseudotime trajectory (B), annotation of states 1, 2, and 3 and percentage of each NPC population in each state (C), and a representation of the *NEUROG2-ASCL1* lineage (D).

(E) Time-lapse imaging of E14.5 double KI cortical explants imaged over 660 min, showing double$^+$ cells (purple arrows) that become Ascl1$^+$ (green arrow) or Neurog2$^+$ (pink arrow), calculated as percentage of double$^+$ NPC conversion (N = 3).

(F) Model of double$^+$ lineage conversion.

(legend continued on next page)

Please cite this article in press as: Han et al., Proneural genes define ground-state rules to regulate neurogenic patterning and cortical folding, Neuron (2021), https://doi.org/10.1016/j.neuron.2021.07.007

baseline (Figure 1I), while Ascl1$^+$ NPCs produced more Pdgfrα^+ oligodendrocytes than pro$^-$ NPCs (Figure 1J). In contrast, double$^+$ NPCs differentiated into neurons and oligodendrocytes above pro$^-$ baseline levels (Figures 1I and 1J). Finally, GFAP$^+$ astrocyte production was highest in the pro$^-$ NPC pool (Figure 1K). We confirmed lineage biases *in vivo*, revealing that *Neurog2*-lineage cells (mCherry$^+$) co-labeled with NeuN (57.4%), a pan-neuronal marker, which was also expressed in double$^+$ lineage cells (42.3%) but was almost negligible in the GFP$^+$, *Ascl1* lineage (5.3%) in postnatal day 2 (P2) double KI cortices (Figure 1L). Instead, Pdgfrα co-labeled Ascl1$^+$ (22.0%) and double$^+$ (15.9%) lineages, while very few Neurog2$^+$ lineage cells were Pdgfrα^+ in P2 double KIs (2.9%; Figure 1M). Finally, for all pro$^+$ populations, few cells co-labeled with S100b, an astrocyte marker (all <2%; Figure 1N). Neurog2$^+$ and Ascl1$^+$ NPCs are thus biased toward neuronal and oligodendrocyte lineages, respectively, while double$^+$ NPCs give rise to either lineage above baseline levels.

Neurog2 and Ascl1 form a cross-repressive toggle switch to control lineage commitment

Single-cell transcriptomic analyses suggest that cortical NPCs undergo a continuum of state transitions before terminal differentiation (Telley et al., 2019). In hematopoiesis, the gradual acquisition of lineage bias is regulated by cross inhibitory TF pairs, which are co-expressed in bipotent progenitors that convert to single TF expression upon lineage bias (Brand and Morrissey, 2020). To test whether *NEUROG2*$^+$*ASCL1*$^+$ NPCs similarly convert to single$^+$ NPCs over time, we examined differentiation trajectories of pro$^+$ cells using scRNA-seq data from 3-mo COs (Figure 2A). In a pseudotime projection, two DCX$^+$ neuronal differentiation trajectories were observed, one dominated by NEUROG2$^+$ cells (state 3) and one by ASCL1$^+$ cells (state 2), each branching off SOX2$^+$ NPCs expressing one or both proneural genes, with double$^+$ NPCs predominant before the lineage branch point (State 1) (Figures 2B–2D and S2A). Consistent with the existence of a cortical-specific *ASCL1* lineage, *ASCL1*$^+$ cells co-expressing interneuron (IN) NPC markers *DLX1/2* or *GSX1/2* were in the minority in 3-mo COs (Figures S2B–S2F). Furthermore, removing *DLX1/2*$^+$ cells from pseudotime projections did not alter differentiation trajectories (Figures S2C–S2F). Finally, to visualize potential conversion events *in vivo*, we performed time-lapse imaging on E14.5 double KI cortical slices (Figure 2E; Video S1), revealing that most mCherry$^+$GFP$^+$ VZ cells converted to mCherry$^+$ (55%; Neurog2$^+$) or GFP$^+$ (33%; Ascl1$^+$) cells over time.

To next determine whether Neurog2 and Ascl1 function as a cross-repressive TF pair (Brand and Morrissey, 2020) (Figure 2F), we first tested dimerization. Neurog2 was initially identified in a two-hybrid screen with Ascl1 as bait (Gradwohl et al., 1996), and accordingly, Neurog2 and Ascl1 co-immunoprecipitated (IP) *in vitro* (Figure 2G) and, using a proximity ligation assay, interacted *in situ* in E12.5 cortical NPCs (Figure 2H). To examine the *in vivo* consequence of Neurog2-Ascl1 interactions, E12.5 cortices were electroporated with a bicistronic pCIG2 vector expressing GFP alone or GFP with *Neurog2*, *Ascl1* (together or separately), or tethered *Neurog2*~*Ascl1*, which forces intramolecular dimerization (Li et al., 2012). *Neurog2* induced the genesis of GFP$^+$Tbr1$^+$ neurons above baseline levels (empty pCIG2) after 24 h, but not when *Neurog2* was co-expressed with or tethered to *Ascl1* (Figure 2I). Conversely, *Neurog2* inhibited *Ascl1* from inducing the formation of Sox9$^+$GFP$^+$ glioblasts, by either tethering or co-expression (Figures 2J and S2G). Finally, we confirmed that Neurog2-Ascl1 inhibitory interactions were transcriptional using reporter assays; *Neurog2* had a reduced ability to transactivate *Neurod1* or *Rnd2* reporters (Li et al., 2012) when co-transfected with *Ascl1*, while *Ascl1* had a reduced ability to transactivate *Dll1-M* (Castro et al., 2006) in the presence of *Neurog2* (Figure 2K). In contrast, a *Dll1* reporter that contained both *Neurog2* and *Ascl1* target sites was transactivated similarly by *Neurog2* and *Ascl1* expressed alone or together (Figure 2K).

Neurog2 and *Ascl1* are thus cross-repressive on lineage-specific genes, providing mechanistic insight into why double$^+$ NPCs, which lie at the apex of a lineage hierarchy, may be less lineage restricted.

Proneural$^-$, Neurog2$^+$, Ascl1$^+$, and double$^+$ cortical NPCs have unique transcriptomes

To elucidate transcriptomic differences that define the four NPC states and explain lineage biases, we performed RNA-seq on E12.5 CD15$^+$ FACS-purified NPCs. Principle-component analysis (PCA) revealed that pro$^-$ and Ascl1$^+$ NPCs were the most divergent, while Neurog2$^+$ and double$^+$ NPCs were the most similar, albeit still distinguishable (Figure 3A). Dissimilarity of the four NPC pools was confirmed using PCA analyses of transcript counts for 114 stem cell genes from a custom Nanostring codeset (Figure S3A; Table S1). Pro$^-$ and Ascl1$^+$ NPCs were enriched in aRG markers (Figures 3B and S3B), while Neurog2$^+$ and double$^+$ NPCs expressed higher levels of glutamatergic neuronal and IPC markers (Figures 3B and S3C–S3E). Notably, Ascl1$^+$ NPCs expressed almost negligible levels of GABAergic and oligodendrocyte markers at E12.5 (Figures S3F and S3G), while astrocyte markers were not detected in any NPCs at E12.5 (RPKM < 1 in all populations). These gene expression profiles mirrored the increased propensity of Neurog2$^+$ and double$^+$ NPCs to differentiate into neurons, while pro$^-$ and Ascl1$^+$ NPCs retained an aRG-like identity at E12.5. Accordingly, of the 1,363 differentially expressed genes (DEGs) signatory of the pro$^+$ NPC phenotype (Figure 3C), many were negative regulators of the cell cycle

(G) Co-immunoprecipitation of Ascl1 with FLAG-Neurog2 with or without DNaseI treatment.
(H) Proximity ligation assay (PLA) of Neurog2 and Ascl1 in E12.5 cortical VZ.
(I and J) E12.5 to E13.5 *in utero* electroporation of pCIG2, *Neurog2*, *Ascl1*, *Neurog2*~*Ascl1* (tethered), or *Neurog2* + *Ascl1*. Quantification of electroporated GFP$^+$ cells that co-express Tbr1 (I) or Sox9 (J) (N = 3 for all).
(K) Transcriptional reporter assays using *Neurod1*, *Rnd2*, *Dll1M*, and *Dll1* luciferase reporters (N = 3 for all).
Data are represented as mean ± SEM. All comparisons made with one-way ANOVA and Tukey's post hoc tests. p values: ns, not significant, *<0.05, **<0.01, ***<0.001. Scale bars in (E), 50 μm; (H), 10 μm; (I), 25 μm. CP, cortical plate; GZ, germinal zone.
See also Figure S2.

Please cite this article in press as: Han et al., Proneural genes define ground-state rules to regulate neurogenic patterning and cortical folding, Neuron (2021), https://doi.org/10.1016/j.neuron.2021.07.007

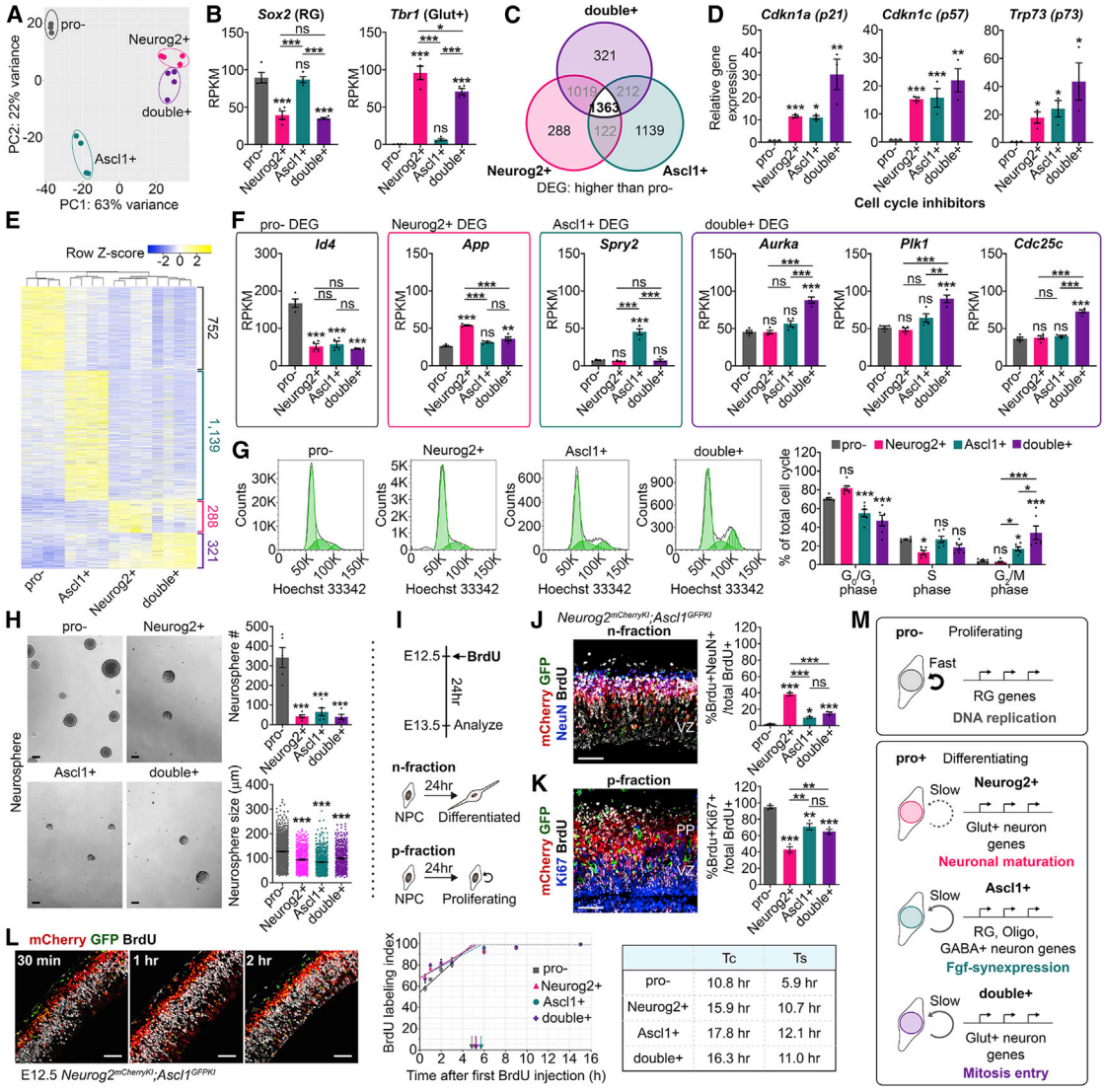

Figure 3. Pro$^-$, Neurog2$^+$, Ascl1$^+$, and double$^+$ cortical NPCs have unique transcriptomes and cell-cycle properties

(A) PCA analysis of RNA-seq data from E12.5 CD15$^+$ NPC pools (N = 4). False discovery rate (FDR) less than 5%.

(B) RPKM values of select markers.

(C) Venn diagram of DEGs >1.5-fold higher in pro$^+$ versus pro$^-$ NPCs (p value < 0.05).

(D) qPCR validation of negative cell-cycle regulators in E12.5 CD15$^+$ NPCs (N = 3), normalizing pro$^-$ NPCs to 1.

(E) Heatmap of DEGs in E12.5 CD15$^+$ NPC pools.

(F) RPKM values of genes enriched in E12.5 CD15$^+$ NPC pools.

(G) Cell-cycle analysis of E12.5 CD15$^+$ NPC pools stained with Hoechst 33342 showing NPCs in G_0/G_1, S, and G_2/M (N = 6).

(H) Primary neurospheres derived from E12.5 CD15$^+$ NPC pools (number, size) after 7 DIV (N = 5).

(I–K) Schematic of n- and p-fraction assay (I). Co-labeling E12.5 double KI cortices with mCherry, GFP, NeuN, and BrdU to calculate n-fraction (%BrdU$^+$NeuN$^+$/BrdU$^+$ cells) (N = 3) (J) and Ki67 and BrdU to calculate p-fraction (%BrdU$^+$Ki67$^+$/BrdU$^+$ cells) (N = 3) (K).

(L) Cumulative BrdU labeling to calculate cell-cycle time (Tc) and S-phase length (Ts) in E12.5 double KIs. Plot of BrdU labeling index (% BrdU$^+$ nuclei, N = 3) and summary of Tc and Ts values. Labeling index saturation points indicated by color-coded arrows for each NPC pool.

(M) Summary of proliferation properties and lineage biases.

Data are represented as mean ± SEM. One-way ANOVA with Tukey's post-hoc tests in (B), (F), (H), (J), and (K), and two-way ANOVA with Tukey's post-hoc test in (G) were used for multiple comparisons. Two-tailed Student's t-tests were used in (D). p-values: ns - not significant, <0.05 *, <0.01 **, <0.001 ***. Scale bars in (H), 100 μm; (J)–(L), 50 μm. Glut$^+$, glutamatergic; GABA$^+$, GABAergic; Oligo, Oligodendrocyte.

See also Figure S3.

Please cite this article in press as: Han et al., Proneural genes define ground-state rules to regulate neurogenic patterning and cortical folding, Neuron (2021), https://doi.org/10.1016/j.neuron.2021.07.007

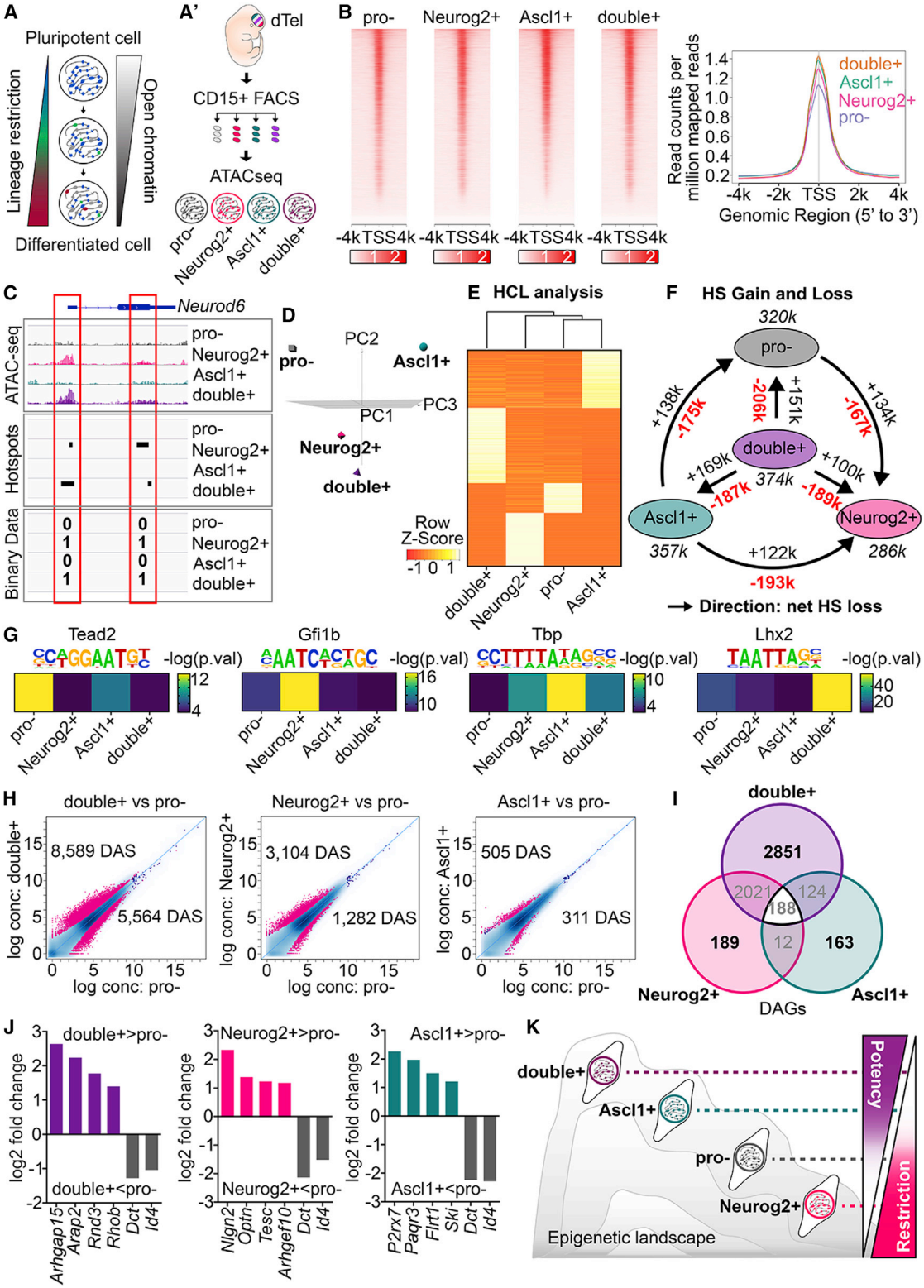

Figure 4. Pro^{-}, Neurog2^{+}, Ascl1^{+}, and double^{+} cortical NPCs have distinct epigenetic landscapes

(A and A′) Gradual acquisition of lineage bias coincident with global loss of open chromatin (A). ATAC-seq of open chromatin in E12.5 CD15^{+} NPC pools (N = 3) (A′).

(B) Heatmap of ATAC-seq TSS peaks in each NPC pool. Read counts per million mapped reads near TSS.

(legend continued on next page)

Please cite this article in press as: Han et al., Proneural genes define ground-state rules to regulate neurogenic patterning and cortical folding, Neuron (2021), https://doi.org/10.1016/j.neuron.2021.07.007

(e.g., *Cdkn1a*, *Cdkn1c*, *Trp73*; Figure S3H). We confirmed the enriched expression of *Cdkn1a*, *Cdkn1c*, and *Trp73* in double$^+$ NPCs by qPCR (Figure 3D), and as expected, we found that the overexpression of these genes in E12.5 NPCs inhibited the formation of primary neurospheres (Figures S3I–S3K).

Finally, we performed an unbiased assessment of uniquely expressed genes in each NPC pool (Figure 3E; Table S2). The 752 DEGs in pro$^-$ NPCs were enriched in Gene Ontology (GO) terms related to proliferation and DNA replication (Figures 3F and S3L), consistent with their higher proliferative potential. The 288 DEGs specific to Neurog2$^+$ NPCs were enriched for GO terms related to neuronal maturation, while the 1,139 Ascl1$^+$-specific DEGs were enriched in GO terms related to various developmental pathways, including MAPK signaling, which regulates Ascl1 activity (Li et al., 2014) (Figures 3F, S3M, and S3N). Finally, of the 321 DEGs enriched in double$^+$ NPCs, several GO terms related to mitosis entry were identified (Figures 3F and S3O). We thus performed cell-cycle profiling using flow cytometric measures of DNA content, revealing a higher proportion of double$^+$ NPCs in G_2/M phase of the cell cycle compared to other NPC pools (Figure 3G), a G_2-pausing phenotype observed in other stem cell types (Sutcu and Ricchetti, 2018). *Neurog2* and *Ascl1* expression thus defines four NPC pools with distinct transcriptomes and cell-cycle kinetics.

Proneural$^+$ NPCs have longer cell cycles and an enhanced propensity to differentiate

Transcriptomic analyses suggested differences in proliferation potential among the four NPC pools, which we tested experimentally using a neurosphere assay to quantify self-renewal/proliferative capacity (Coles-Takabe et al., 2008). CD15$^+$ NPCs were plated at clonal density, and after 7 days *in vitro* (DIV), pro$^-$ NPCs formed an order of magnitude more neurospheres that were also larger in size than pro$^+$ NPCs, which gave rise to fewer and smaller neurospheres (Figure 3H). Notably, as proneural gene expression is perturbed by *in vitro* culture (Neurog2-OFF, Ascl1-ON) (Li et al., 2014), secondary and tertiary neurospheres from each group no longer showed differences between the NPC pools (Figure S3P).

To further assess the association between proneural gene expression and NPC fate choice, we calculated neurogenic (n) and proliferative (p) fractions *in vivo* in E12.5 double KI mice (Figure 3I). In pro$^-$ NPCs, the n-fraction (%BrdU$^+$NeuN$^+$/BrdU$^+$) and q-fraction (%BrdU$^+$Ki67$^-$/BrdU$^+$), a measure of cell-cycle leaving, were negligible, suggesting that pro$^-$ NPCs have a lower probability to differentiate (Figures 3J and S3Q). In contrast, >30% of all pro$^+$ NPCs exited the cell cycle, with Neurog2$^+$ NPCs the most likely to undergo neurogenesis (Figures 3J and S3Q). Conversely, p-fractions were highest in pro$^-$ NPCs (% BrdU$^+$Ki67$^+$/BrdU$^+$ cells), confirming a bias to stay in the cell cycle, while p-fractions were lower in all pro$^+$ NPCs, especially the Neurog2$^+$ NPC pool (Figure 3K). Finally, using cumulative BrdU labeling (Figure 3L), we found that total cell cycle (Tc) and S-phase (Ts) lengths were longer in pro$^+$ NPCs versus pro$^-$ NPCs but were not different from one another (Figure 3L), consistent with cell-cycle length increases in differentiating NPCs (Dalton, 2015). Pro$^+$ NPCs thus have longer cell-cycle lengths that are conducive to differentiation, but only a subset of pro$^+$ NPCs differentiate at any given time, with singular Neurog2 expression the best determinant of cell-cycle exit (Figure 3M).

Proneural$^-$, Neurog2$^+$, Ascl1$^+$, and double$^+$ NPCs display differences in chromatin accessibility

NPCs undergo semi-stable cell-fate transitions that increasingly restrict lineage potential (Telley et al., 2019). Fate restriction is accompanied by closure of chromatin sites associated with multipotency and opening of sites where lineage-specifying TFs bind (Stergachis et al., 2013) (Figure 4A). Using ATAC-seq, we performed a genome-wide comparison of "open" chromatin sites in E12.5 CD15$^+$ NPC pools (Figure 4A'). Open transcription start sites (TSSs) were most abundant in double$^+$ NPCs, followed by Ascl1$^+$, Neurog2$^+$, and pro$^-$ NPCs (Figure 4B). However, as chromatin is also extensively reorganized outside TSSs (Dixon et al., 2015), we also interrogated genome-wide differences using a hotspot (HS) algorithm (John et al., 2011) (Figure 4C). PCA revealed that double$^+$ and Neurog2$^+$ NPCs had the most similar DNA regulatory landscapes, and Ascl1$^+$ and pro$^-$ NPCs were most divergent (Figure 4D). Strikingly, hierarchical clustering (HCL) analysis for gene-assigned HSs showed distinct, almost non-overlapping sites of open chromatin in each NPC pool, with double$^+$ NPCs the most divergent (Figure 4E). Furthermore, an analysis of all HSs, whether gene assigned or not, revealed the highest HS number in double$^+$ NPCs (374,000) (Figure 4F), recapitulating the total TSS peak comparisons (Figure 4B). However, pro$^-$ NPCs (320,000) had more HSs compared to Neurog2$^+$ NPCs (286,000), opposite to the TSS peaks, indicating that even though Neurog2$^+$ NPCs had fewer sites of open chromatin, more of these sites were in TSSs (Figure 4F).

Increased open chromatin is associated with multipotency, while reduced chromatin accessibility is associated with a transition to a more lineage-restricted state (Stergachis et al., 2013). We queried lineage restriction by examining HS gain (+) and loss (–) in pairwise comparisons (arrow depicts direction HS loss > HS gain; Figure 4F), following the assumption that more HS are lost than gained during lineage restriction (Stergachis et al., 2013). For example, of 374,000 HSs in double$^+$ NPCs, 187,000 were "lost" or not present in Ascl1$^+$ NPCs, which instead acquired 169,000 new HSs, for a total of 357,000 HS. Double$^+$ NPCs lost more HSs than they gained in this and in all three pairwise comparisons, meaning that they retained the most open

(C–F) HS analysis to quantitate ATAC-seq data, showing *Neurod6* locus (C). PCA of high-confidence HSs present in all three biological replicates for each NPC pool (D). Hierarchical clustering of gene-assigned HSs in each NPC pool (E). HS gain and loss in pairwise comparisons (F). Arrows show direction of net HS loss, suggestive of lineage restriction.

(G) HOMER motif analysis showing top rank motifs in each NPC pool.

(H–J) Diffbind analysis of ATAC-seq data showing DAS in pairwise comparisons between NPC pools (H). Venn diagram comparing differentially accessible genes (DAGs) in pro$^+$ versus pro$^-$ NPC pools (I). Fold differences in open chromatin for select gene sets, comparing pro$^-$ versus pro$^+$ NPCs (J).

(K) Epigenetic landscape model depicting lineage restriction based on comparison of open chromatin sites.

See also Figure S4.

Please cite this article in press as: Han et al., Proneural genes define ground-state rules to regulate neurogenic patterning and cortical folding, Neuron (2021), https://doi.org/10.1016/j.neuron.2021.07.007

CellPress

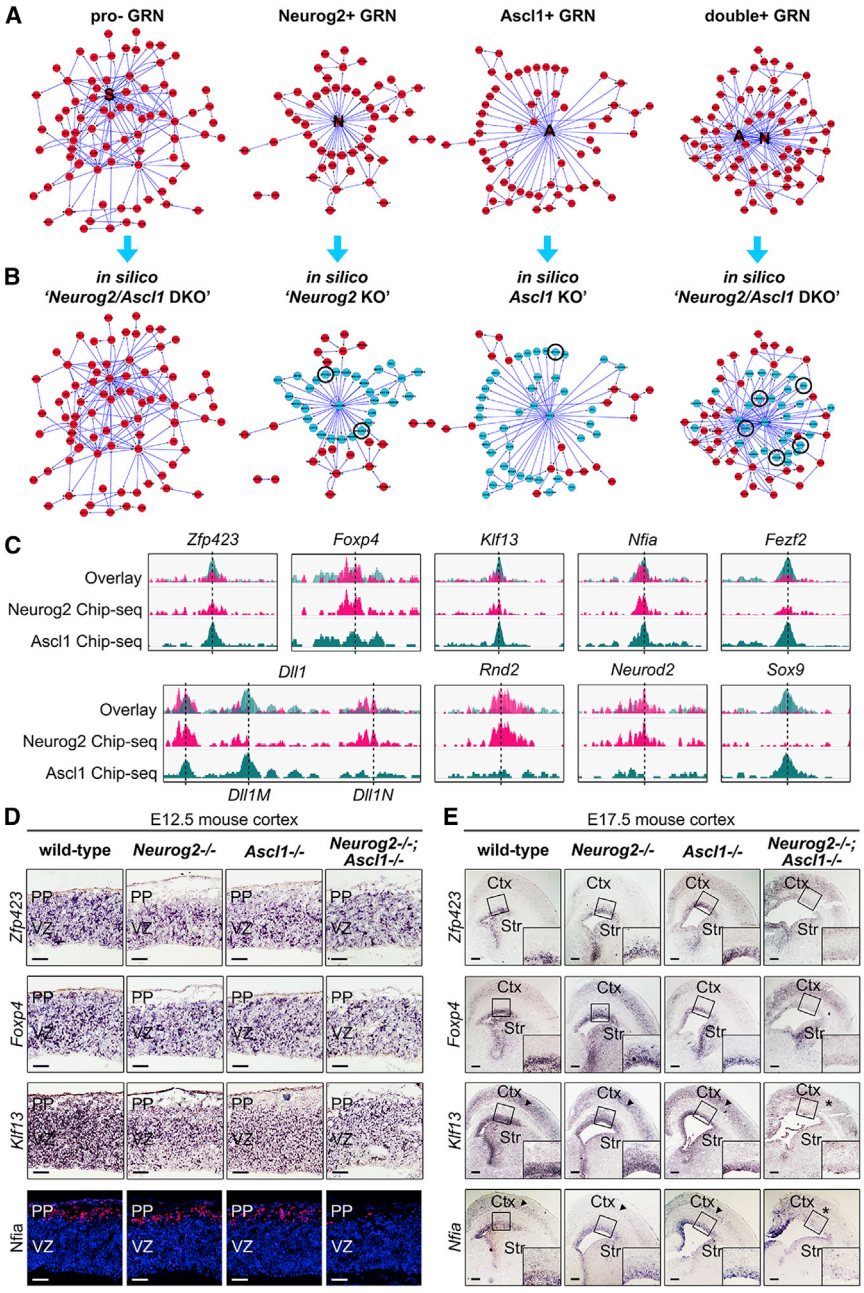

Figure 5. *In silico* and *in vivo* analyses of GRNs associated with pro$^-$, Neurog2$^+$, Ascl1$^+$, and double$^+$ cortical NPCs

(A) GRNs associated with E12.5 CD15$^+$ NPC pools.

(B) *In silico* "*Neurog2/Ascl1* DKO" effects on the pro$^-$ GRN, "*Neurog2* KO" on the Neurog2$^+$ GRN, "*Ascl1* KO" on the Ascl1$^+$ GRN, and "*Neurog2/Ascl1* DKO" on the double$^+$ GRN. Blue nodes depict predicted loss of gene expression. Genes selected for further analysis are circled.

(C) Neurog2 and Asc1l ChIP-seq peaks for genes in double$^+$ GRN; *Zfp423*, *Foxp4*, *Klf13*, and *Nfia* and known common targets, *Fezf2* and *Dll1*; Neurog2 targets, *Rnd2* and *Neurod2*; and an Ascl1 target, *Sox9*.

(D and E) Expression of predicted Neurog2/Ascl1 target genes, *Zfp423*, *Foxp4*, *Klf13*, and *Nfia* in E12.5 (D) and E17.5 (E) wild-type, *Neurog2*$^{-/-}$, *Ascl1*$^{-/-}$, and DKO cortices. Insets are 2× magnifications of boxed regions.

Scale bars in (D), 50 μm; (E), 200 μm. Str, striatum. See also Figure S5.

chromatin, a hallmark of a less lineage-restricted state (Figure 4F). Conversely, Neurog2$^+$ NPCs had fewer HSs than all comparators, consistent with increased fate restriction, while pro$^-$ (net loss in two comparisons) and Ascl1$^+$ (net loss in one comparison) NPCs had intermediate phenotypes (Figure 4F).

Next, to identify TFs that could convey unique features of each NPC pool, we performed HOMER motif analysis. p value rankings identified Tead2, Gfi1b, Tbp, and Lhx2 binding motifs as the most enriched ($-\log(\text{p value}) > 1.5$) in open chromatin of pro$^-$, Neurog2$^+$, Ascl1$^+$, and double$^+$ NPCs, respectively (Figure 4G; Table S3). Finally, we applied a Diffbind analysis to identify differential accessible sites (DASs) and differential accessible genes (DAGs). In pairwise comparisons to pro$^-$ NPCs, double$^+$ NPCs had the most DASs (FDR < 0.10), followed by Neurog2$^+$ and Ascl1$^+$ NPCs (Figure 4H; Table S4). Within the DASs, double$^+$ NPCs had an order of magnitude more DAGs (2,851 total), which were similar in number in all other NPC pools (ranging from 64 to 189), consistent with a potential for genes in multiple lineages/pathways to be transactivated in double$^+$ NPCs (Figures 4I, 4J, and S4A–S4E).

Our data support a continuum of lineage restriction, from lowest to highest: double$^+$< Ascl1$^+$< pro$^-$< Neurog2$^+$ NPC, with double$^+$ NPCs least lineage restricted and Neurog2$^+$ NPCs poised to differentiate (Figure 4K).

Double$^+$ gene regulatory networks are deregulated in *Neurog2*$^{-/-}$;*Ascl1*$^{-/-}$ cortices

GRNs can be used to identify central genes that uphold networks associated with unique cell states. To visualize critical GRNs that uphold cortical NPC states, we combined RNA-seq, ATAC-seq, and *in vivo* Neurog2 (Sessa et al., 2017) and Ascl1 (this study) ChIP-seq datasets (Figure 5A) (Okawa et al., 2015). *Neurog2* and *Ascl1* formed central hubs in their respective GRNs and in the double$^+$ GRN, whereas *Sox2* formed a central regulatory hub in pro$^-$ GRNs (Figure 5A; Table S5).

To understand how *Neurog2* and *Ascl1* sustain cell identities, we performed *in silico* perturbations to identify proneural gene-dependent GRN hubs (Figure 5B; Table S5). As expected, the pro$^-$ GRN was not affected by *Neurog2* knockout (KO) or *Ascl1* KO simulations as these genes are not present. Conversely, single KO simulations were disruptive on their

Please cite this article in press as: Han et al., Proneural genes define ground-state rules to regulate neurogenic patterning and cortical folding, Neuron (2021), https://doi.org/10.1016/j.neuron.2021.07.007

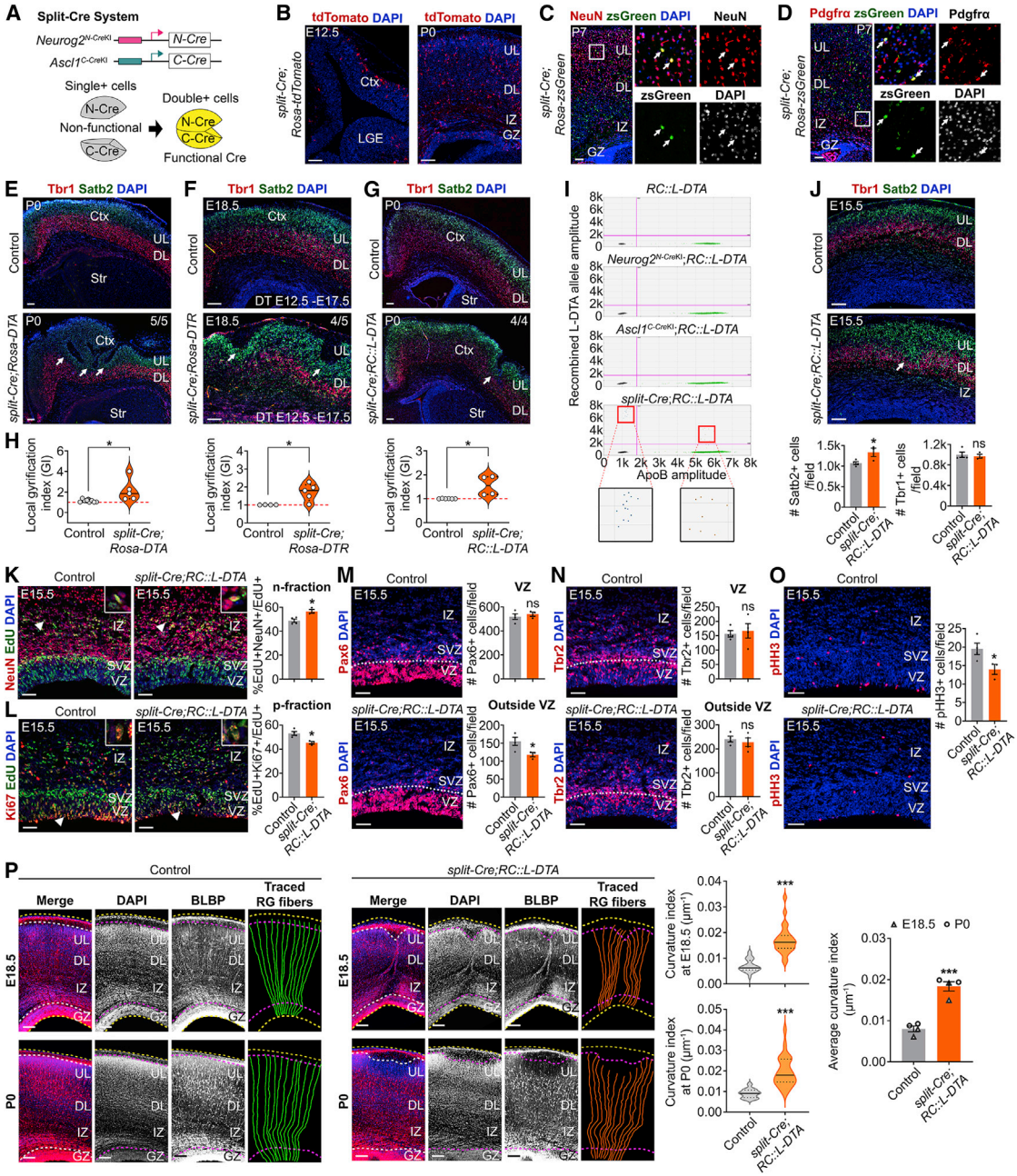

Figure 6. Double$^+$ NPCs are essential to sustain regular neurogenesis and prevent cortical folding

(A) Knockin strategy to generate split-Cre transgenics.

(B–D) Lineage tracing in E12.5 and P0 *split-Cre;Rosa-tdTomato* cortices (B) and P7 *split-Cre;Rosa-zsGreen* cortices, showing co-staining of reporters with NeuN (C) and Pdgfrα (D). Insets are 4× magnifications. Arrows mark double$^+$ cells.

(E–H) Tbr1/Satb2 immunolabeling of P0 control (N = 8) and split-Cre;Rosa-DTA (N = 5) cortices (E), E18.5 control (N = 4) and *split-Cre;Rosa-DTR* (N = 5) cortices after DT injection from E12.5 to E17.5 (F), and P0 control (N = 6) and *split-Cre;RC::L-DTA* (N = 4) cortices (G). Arrows mark cortical folds. Penetrance of folding phenotype indicated in upper right corner. Quantification of gyrification indices (H).

(I) ddPCR analysis of genomic DNA from single Cre$^+$ and *split-Cre;RC::L-DTA* P0 retinas. Insets are 3× magnifications of boxed regions.

(J) Tbr1$^+$ and Satb2$^+$ neuron counts in E15.5 control (N = 4) and *split-Cre;RC::L-DTA* (N = 3) cortices.

(K and L) Calculation of n-fraction (K) and p-fraction (L) in E15.5 control (N = 4) and *split-Cre;RC::L-DTA* (N = 3) cortices.

(M–P) Expression and quantification of Pax6$^+$ (M), Tbr2$^+$ (N), and pHH3$^+$ (O) cells inside and outside the VZ in E15.5 control (N = 4) and *split-Cre;RC::L-DTA* (N = 3) cortices. BLBP immunostaining of E18.5/P0 control and *split-Cre;RC::L-DTA* cortices (N = 4 total; 2 each stage, with n = 13 fibers traced per brain) (P). Representative aRG fiber tracings are shown. Quantification of curvature index of individual aRG fibers.

(legend continued on next page)

Please cite this article in press as: Han et al., Proneural genes define ground-state rules to regulate neurogenic patterning and cortical folding, Neuron (2021), https://doi.org/10.1016/j.neuron.2021.07.007

corresponding GRNs; the Neurog2$^+$ GRN lost 58.5% of total nodes in a simulated *Neurog2* KO and the Ascl1$^+$ GRN lost 70.0% of all nodes in an *Ascl1* KO (Figure 5B), whereas single KO simulations had less effect on the double$^+$ GRN (17.4% total nodes lost by *Neurog2* KO and 8.7% of total nodes lost by *Ascl1* KO; Figure S5A; Table S5). Instead, the double$^+$ GRN lost the most total nodes (44.9%) in a simulated *Neurog2*/*Ascl1* double KO (DKO) (Figure 5B).

To determine whether deregulated genes in the double$^+$ GRN identified *in silico* were common targets of Neurog2 and Ascl1, we examined ChIP-seq peaks. Overlapping Neurog2/Ascl1 ChIP-seq peaks were found in double$^+$ GRN genes predicted to be perturbed in double KOs, such as *Zfp423*, *Foxp4*, *Klf13*, and *Nfia*, as well as in two known genes co-regulated by Neurog2 and Ascl1, *Fezf2* (Dennis et al., 2017) and *Dll1* (Castro et al., 2006) (Figure 5C). Conversely, known Neurog2-specific target genes (*Rnd2*, *Neurod2*, *Dll1-N*) and Ascl1-specific target sites (*Sox9*, *Dll1-M*) (Castro et al., 2006) showed binding preferences to one proneural TF (Figure 5C).

Finally, to validate *in silico* GRN disruptions *in vivo*, we examined the expression of putative deregulated genes in E12.5 *Neurog2*/*Ascl1* single KO and DKO cortices. At E12.5, *Zfp423*, *Foxp4*, and *Klf13* were expressed in the cortical VZ and were not noticeably perturbed in single KOs or DKOs, whereas GRN genes expressed in the cortical preplate, *Nfia* and *Bhlhe22*, were downregulated only in DKOs (Figures 5D and S5B). At E17.5, *Nfia* and *Klf13* were downregulated in DKO cortical neurons, similar to the reported loss of *Fezf2* expression in layer V (Dennis et al., 2017), and *Zfp423*, *Foxp4*, *Klf13*, and *Nfia* were all downregulated in the DKO germinal zone (GZ) (Figure 5E). However, GZ effects were difficult to interpret given that Pax6$^+$ and Sox9$^+$ aRG and Tbr2$^+$ IPCs were depleted in E17.5 DKO cortices (Figures S5C–S5E). Nevertheless, these data support the idea that Neurog2 and Ascl1 co-regulate a subset of distinct genes within a unique GRN.

Double$^+$ NPCs are required for neurogenic symmetry and cortical lissencephaly

To ask whether double$^+$ NPCs have an important role *in vivo*, we developed a split-Cre system (Hirrlinger et al., 2009), knocking N- and C-Cre termini into *Neurog2* (*Neurog2$^{N\text{-}CreKI}$*) and *Ascl1* (*Ascl1$^{C\text{-}CreKI}$*) loci, respectively, such that full-length Cre was reconstituted only in double$^+$ NPCs (Figure 6A). We confirmed half *Cre* expression in *Neurog2*$^+$ or *Ascl1*$^+$ NPCs in E12.5 cortices from the respective lines using RNAscope (Figure S6A). To trace double$^+$ NPC progeny, *Neurog2$^{N\text{-}CreKI}$;Ascl1$^{C\text{-}CreKI}$* (hereafter *split-Cre*) mice were crossed with *Rosa* reporters. At E12.5 and P0, recombined tdTomato$^+$ cells were scattered through the preplate and cortical plate, respectively (Figure 6B). At P7, zsGreen$^+$ cells co-labeled with NeuN (neurons) and Pdgfrα (oligodendrocytes) (Figures 6C and 6D), confirming the bipotency of double$^+$ NPCs, also observed in short-term lineage tracing (Figure 1).

To assess the requirement for double$^+$ NPCs, we deleted these cells by crossing split-Cre mice with three Cre-dependent, transgenic "deleter" lines. Both *Rosa-DTA* and *RC::L-DTA* mice express *diphtheria toxin (DT) subunit A (DTA)* in a Cre-dependent fashion, the latter with an inverted *DTA* gene to prevent leaky expression (Plummer et al., 2017). *Rosa-DTR* mice induce cell death when DT, which we administered daily from E12.5 to E17.5, is taken up, driving Cre-dependent expression of the *DT receptor (DTR)*. Strikingly, deep cortical folds affecting upper Satb2$^+$ and lower Tbr1$^+$ neuronal layers formed in random locations in all three *split-Cre;deleter* strains, with local gyrification indices (GI) > 1, indicative of cortical folding (Figures 6E–6H and S6B–S6D). Using droplet digital PCR (ddPCR), we confirmed that these defects correlated with Cre-mediated recombination, as the *RC::LC-DTA* allele was recombined only when both Cre alleles were present (Figure 6I).

To understand how cortical folding first arises, we examined E15.5 *split-Cre;RC::L-DTA* cortices, confirming DTA toxicity by increased TUNEL labeling (Figure S6E). Strikingly, more Satb2$^+$ upper-layer neurons developed in E15.5 *split-Cre;RC::L-DTA* (Figure 6J) and E15.5 and P0 *split-Cre;Rosa-DTA* (Figures S6F and S6G) cortices, while Tbr1$^+$ neurons were present in normal numbers. There was also a global increase in the number of NPCs differentiating into neurons (n-fraction) and a reduction in NPCs staying in cycle (p-fraction) in *split-Cre;RC::L-DTA* cortices assayed from E14.5 to E15.5 (Figures 6K and 6L). Upper-layer neuronal expansion is associated with the appearance of bRG in gyrencephalic cortices (Wang et al., 2011). However, the total number of Pax6$^+$ aRG and Tbr2$^+$ IPCs did not change in E15.5 *split-Cre;RC::L-DTA* cortices (Figures 6M and 6N), and instead, there were fewer total pHH3$^+$ NPCs and less basal Pax6$^+$ NPCs outside the VZ (Figures 6M and 6O).

In human and non-human primate cortices, with the onset of upper-layer neurogenesis, aRG lose their pial contacts to become truncated RG (Nowakowski, 2016), with bRG instead supporting migration along a trajectory that is now curved because of the asymmetric insertion of bRG into the glial scaffold (Llinares-Benadero and Borrell, 2019). Using brain lipid-binding protein (BLBP) to label aRG, we evaluated process trajectories in E18.5/P0 *split-Cre;RC::L-DTA* mice, revealing an increased curvature at both stages and a premature retraction of glial processes from the pial surface at P0 at sites of cortical folding (Figure 6P). Notably, aRG deformities developed even though the basement membrane remained intact (Figure S6H). Altogether, deletion of double$^+$ NPCs results in the production of more upper-layer neurons and cortical folding correlates with a curvature of the radial glial scaffold and not bRG expansion.

Double$^+$ NPCs regulate Notch signaling

The striking cortical folding phenotype was unexpected given that so few cortical NPCs are double$^+$, leading us to consider non-cell-autonomous effects. Proneural TFs promote differentiation cell autonomously and induce neighboring NPCs to proliferate non-cell autonomously by transactivating *Dll1* and *Dll3* ligands to initiate Notch signaling (Castro et al., 2006). Strikingly, from our RNA-seq data, *Dll1* and *Dll3* were expressed at the highest levels

Data are represented as mean ± SEM. Two-tailed Student's t tests were used in (H) and (J)–(P). p values: ns, not significant, *<0.05, **<0.01, ***<0.001. Scale bars in (B)–(G), (J), and (P), 100 μm; (K)–(O), 50 μm.
See also Figure S6.

Please cite this article in press as: Han et al., Proneural genes define ground-state rules to regulate neurogenic patterning and cortical folding, Neuron (2021), https://doi.org/10.1016/j.neuron.2021.07.007

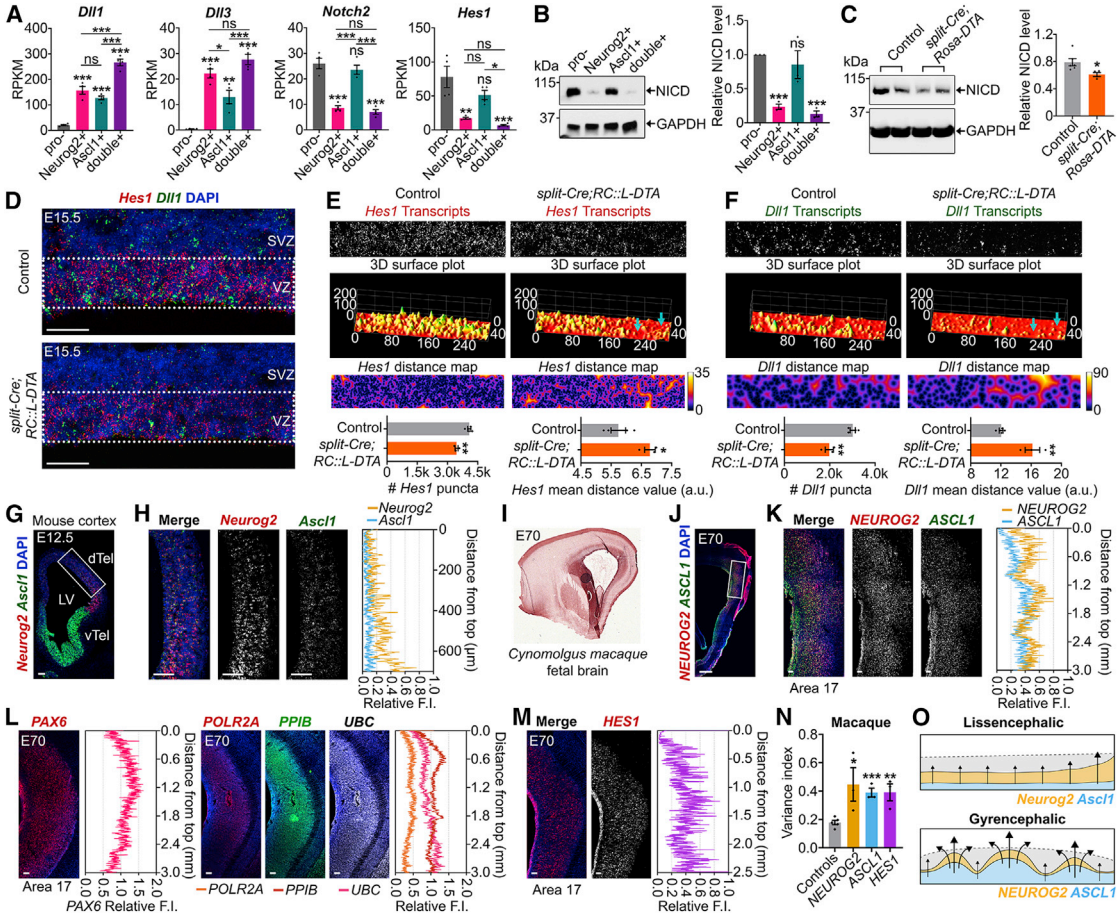

Figure 7. Double$^+$ NPCs are Notch-ligand-expressing niche cells that are distributed evenly in mouse cortices and modular in gyrencephalic species

(A) RPKM values from RNA-seq data from E12.5 CD15$^+$ NPC pools (N = 4).

(B and C) Western blots and densitometry of NICD in E12.5 CD15$^+$ NPC pools (N = 3), normalized to GAPDH and to pro$^-$ NPCs (set at 1) (B), and in P0 control (N = 6) and split-Cre;Rosa-DTA cortices (N = 4), normalized to GAPDH (C).

(D–F) *Hes1* and *Dll1* transcript distribution in E15.5 control (N = 4) and split-Cre;Rosa-DTA (N = 3) cortices (D). Grayscale plot and 3D surface plot for *Hes1* (E) and *Dll1* (F) transcripts. Reduction in *Hes1* and *Dll1* signals indicated by blue arrows. Quantification of *Hes1* and *Dll1* puncta and mean distance values.

(G–N) *Neurog2* and *Ascl1* transcript distribution in E12.5 mouse cortex (G), showing 3× magnification (H). Parasagittal section of E70 macaque cortex (I). RNAscope analysis of *NEUROG2* and *ASCL1* in P70 macaque cortex (J), showing 4× magnification of boxed area 17 and a relative fluorescence intensity (FI) plot normalized to DAPI (K). RNAscope analysis of control (*PAX6*, *POLR2A*, *PPIB*, *UBC*) (L) and *HES1* (M) transcripts in area 17 visual cortex of E70 macaque, showing 3× magnification and normalized FI plots. Quantification of variance indices for controls (*PAX6*, *POLR2A*, *PPIB*, *UBC*, *HOPX*), *NEUROG2*, *ASCL1*, and *HES1* (N = 3) transcripts (N).

(O) Model of Neurog2/Ascl1 influence on cortical folding.

Data are represented as mean ± SEM. One-way ANOVA with Tukey's post hoc tests were used for multiple comparisons in (A). Two-tailed Student's t tests were used in (B), (C), (E), (F), and (N). p values: ns, not significant, *<0.05, **<0.01, ***<0.001. Scale bars in (D), 50 μm; (G), (H), and (K)–(M), 100 μm; (J), 1 mm. dTel, dorsal telencephalon; GZ, germinal zone; LV, lateral ventricle: vTel, ventral telencephalon.

in Neurog2$^+$ and double$^+$ NPCs, while the *Notch2* receptor and two downstream effectors, *Hes1* and the Notch intracellular domain (NICD), were all elevated in pro$^-$ and Ascl1$^+$ NPCs (Figures 7A and 7B).

The heterogeneity of Notch signaling in the four NPC pools suggested that removal of a critical source of Notch ligands (i.e., double$^+$ NPCs) could disrupt signaling. Indeed, overall NICD levels were reduced in P0 *split-Cre;Rosa-DTA* cortices (Figure 7C). To examine the spatial pattern of Notch signaling, we examined the geometry of *Hes1* and *Dll1* transcript distribution using RNAscope. While there were fewer *Hes1* (Figures 7D and 7E) and *Dll1* (Figure 7F) mRNA puncta in E15.5 *split-Cre;RC::L-DTA* cortices, more telling was the increased spatial distancing between puncta as revealed by 3D surface plots, indicative of a sporadic disruption of Notch signaling (Figures 7E and 7F). Double$^+$ NPCs thus act as essential Notch-ligand-expressing niche cells that are required to sustain homogeneous patterns of Notch signaling.

Please cite this article in press as: Han et al., Proneural genes define ground-state rules to regulate neurogenic patterning and cortical folding, Neuron (2021), https://doi.org/10.1016/j.neuron.2021.07.007

Proneural$^+$ NPCs are uniformly distributed in lissencephalic and modular in gyrencephalic cortices

To test whether *Neurog2* and *Ascl1* expression profiles differ in lissencephalic (rodent) versus gyrencephalic (primate) cortices, we used RNAscope to examine transcript periodicity. In E12.5 murine cortices, *Neurog2* and *Ascl1* transcripts were distributed evenly across the VZ, with higher expression laterally (Figures 7G and 7H), which is developmentally more mature. In area 17 of the E70 macaque visual cortex, midway during neurogenesis, the germinal zone was histologically "smooth," whereas *NEUROG2*, *ASCL1*, and *HES1* transcripts had a modular distribution, with areas of high expression separated by lower expression, supported by an increased variance index (Figures 7I–7N and S7). In contrast, *PAX6*, *HOPX*, and three ubiquitously expressed control genes had relatively continuous expression across the area 17 germinal zone (Figures 7L, 7N, and S7). *Neurog2*, *Ascl1*, and *Hes1* mRNA, a Notch effector, are thus uniformly distributed in smooth cortices and modular in folded cortices (Figure 7O), consistent with a proneural gene-regulated, Notch-driven process driving cortical folding.

DISCUSSION

Cortical folding has evolved independently several times during evolution (Lewitus et al., 2013). A major contributing force is bRG expansion, which produces more upper-layer neurons and complexifies neuronal migratory routes in gyrencephalic cortices (Del Toro et al., 2017; Llinares-Benadero and Borrell, 2019). However, a global increase in basal NPCs alone does not induce cortical folding in rodents (Nonaka-Kinoshita et al., 2013) unless increases are focal (Rash et al., 2013; Stahl et al., 2013). Here, we report that cortical folding can occur without bRG expansion and can instead be achieved if neurogenesis and/or aRG trajectories are discontinuous.

Our data support a role for double$^+$ NPCs as Notch-ligand-expressing niche cells that are essential to maintain neurogenic continuity and prevent cortical folding in rodents, providing a functional link between Notch signaling and gyrencephaly. Notch has been previously identified as a niche signal in the adult brain, with Notch ligands (Jag1) expressed by endothelial cells required to maintain NSC quiescence and prevent neuronal differentiation (Ottone et al., 2014). Similarly, Notch is required for the spatiotemporal regulation of adult NSC activity in zebrafish (Dray et al., 2021). Given our finding that Notch signaling is differentially active in specific subsets of cortical NPCs during development and that the selective removal of double$^+$, Notch-ligand-expressing NPCs has striking defects on cortical morphology, we provide support for Notch as a niche cell signal in the embryonic cortex. Furthermore, consistent with proneural TF-regulated Notch signaling playing a niche-like role in gyrencephalic species, we found that *NEUROG2*, *ASCL1*, and *HES1* transcripts have a modular distribution in the macaque cortex, as observed for other neurogenesis genes in ferret (de Juan Romero et al., 2015). Intriguingly, a human-specific *NOTCH2NL* gene is expressed in cortical RG and, when overexpressed, blocks neurogenesis, although a role in folding could not be assessed with the CO system employed (Fiddes et al., 2018). However, we propose that the increased proportion of double$^+$ NPCs in human and NHP cortices may lead to a more fine-tuned regulation of Notch signaling, controlling the position and/or depths of cortical folds in gyrencephalic cortices.

How progenitor cells gradually become lineage restricted has been carefully dissected in hematopoiesis, in which several TF pairs maintain bipotency through mutual cross-repression at lineage branch points (Brand and Morrissey, 2020; Palii et al., 2019). A computational model of stem and progenitor cell maintenance suggests that the balance of opposing differentiation forces is regulated by cross-repressive TF pairs, which prime cells for lineage selection (Okawa et al., 2016). In a 2009 review (Graf and Enver, 2009), the authors proposed that most lineage branch points would be regulated by cross-repressive TFs, a model that has since gained experimental support in embryonic stem cells (ESCs) (Dillon, 2012) and pancreatic (Collombat et al., 2003) and dermomyotome (Lagha et al., 2009) development. Our finding that Neurog2 and Ascl1 are a cross-repressive TF pair that function at a lineage bifurcation point provides evidence that a similar mode of lineage priming occurs in the nervous system. Neurog2 and Ascl1 cross-repression is likely achieved by heterodimerization, as these two bHLH TFs recognize distinct E boxes (Aydin et al., 2019; Raposo et al., 2015; Wapinski et al., 2013), and we found that heterodimers have a reduced ability to transactivate lineage-specific target genes. However, Neurog2 and Ascl1 also have common targets that may play a critical role in maintaining double$^+$ NPC bipotency (our study and Aydin et al., 2019; Masserdotti et al., 2015). The finding that Lhx2 binding sites are enriched in open chromatin regions of double$^+$ NPCs is of particular interest, as *Lhx2* regulates NPC proliferation and regionalized NSC gene expression (Chou and O'Leary, 2013; Hagey et al., 2016). Moreover, *Lhx2* and *Lhx9* are important temporal regulators of cortical neurogenesis (Peukert et al., 2011).

Cell-fate decisions are not only dictated by the repertoire of TFs expressed but also by the chromatin landscape. In neural lineages, Neurog2 and Ascl1 are pioneer factors that bind closed chromatin and facilitate opening of these sites (Aydin et al., 2019; Wapinski et al., 2013). Based on the amount of open chromatin, we ordered double$^+$, Ascl1$^+$, pro$^-$, and Neurog2$^+$ NPCs from highest to lowest, which correlated with differentiation biases *in vitro* and *in vivo*. Notably, the lack of a complete restriction to one lineage or the other was expected as lineage biases gradually accumulate before ultimately culminating in cell-fate selection (Brand and Morrissey, 2020). Lineage biases of Neurog2$^+$, Ascl1$^+$, and pro$^-$ NPCs toward neuronal, oligodendrocyte, and astrocyte differentiation, respectively, were consistent with prior studies of individual genes (Li et al., 2012, 2014; Parras et al., 2007), but the bipotency of double$^+$ NPCs was an unexpected finding.

Pro$^+$ NPCs had longer cell cycles than pro$^-$ NPCs, which is associated with differentiation, while conversely, increased pluripotency is associated with G_1 and G_2 shortening (Dalton, 2015). We observed S-phase lengthening in all pro$^+$ versus pro$^-$ NPCs, similar to an increased S-phase length in Ascl1$^+$ NPCs in the adult SVZ (Ponti et al., 2013). Notably, global chromatin remodeling occurs in S phase, when cell-fate restriction occurs (Ma et al., 2015). We also provide evidence for G_2 pausing in double$^+$ NPCs, which is linked to stem cell maintenance in the zebrafish myotome, Hydra embryo, and "super-healer" mice (Sutcu and

Please cite this article in press as: Han et al., Proneural genes define ground-state rules to regulate neurogenic patterning and cortical folding, Neuron (2021), https://doi.org/10.1016/j.neuron.2021.07.007

Ricchetti, 2018). Cells paused in G_2 are thought to have passed the energy-consuming DNA replication step and are poised to quickly undergo mitosis and differentiate. Double$^+$ NPCs express the highest levels of *Cdkn1a*, a known G_2-pausing factor (Bunz et al., 1998), as well as *Cdkn1c* and *Trp73*, all of which are required for long-term maintenance of NSCs (Furutachi et al., 2015; Kippin et al., 2005; Talos et al., 2010).

In summary, by stratifying the cortical NPC pool based on Neurog2 and Ascl1 expression, we have gained unprecedented new insights into how cortical folding is controlled, revealing a role for double$^+$ NPCs as Notch-ligand-producing niche cells. Future studies using scRNA-seq with high read counts may reveal an even deeper level of double$^+$ NPC heterogeneity and new functional insights into the roles that these cells play during cortical development.

STAR★METHODS

Detailed methods are provided in the online version of this paper and include the following:

- KEY RESOURCES TABLE
- RESOURCE AVAILABILITY
  - Lead Contact
  - Materials Availability
  - Data and Code Availability
- EXPERIMENTAL MODELS AND SUBJECT DETAILS
  - Mice
  - Non-human primates
  - Human cerebral organoids
- METHOD DETAILS
  - *In utero* electroporation
  - Injection of Diphtheria toxin
  - Sectioning and immunohistochemistry
  - BrdU staining and cell cycle analyses
  - RNA *in situ* hybridization
  - RNAscope assay
  - Time lapse imaging
  - Fluorescence activated cell sorting (FACS) and flow cytometry
  - Neurosphere assay
  - Directed differentiation assay
  - Nucleofection
  - TUNEL assay
  - EdU Click it assay
  - Luciferase Assays
  - Immunoprecipitation (IP)
  - Western blot
  - Proximity Ligation Assay (PLA)
  - RNA-seq
  - Nanostring analysis
  - RT-qPCR
  - ATAC-seq
  - ChIP seq
  - Gene regulation network analysis (GRN) and *in silico* perturbation assay
  - scRNA-seq data analysis of human COs and fetal cortices
  - Droplet digital PCR
- QUANTIFICATION AND STATISTICAL ANALYSIS
  - Imaging and image processing methods
  - Identification of VZ and non VZ
  - Calculation of local gyrification index (GI)
  - Curvature analysis of radial glia (RG) trajectories
  - Analysis of Variance Indices

SUPPLEMENTAL INFORMATION

Supplemental information can be found online at https://doi.org/10.1016/j.neuron.2021.07.007.

ACKNOWLEDGMENTS

We thank Marjorie Brand, Magdalena Götz, and François Guillemot for critical comments and Petia Stefanova, Yutaka Amemiya (SRI), Andrey Golubov (U of Lethbridge), and Ying Liu (Applied Organoid Core, U of T) for technical help. This work was supported by a Canadian Institutes of Health Research (CIHR PJT – 162108) operating grant to C.S. and I.K., Canada-Israel Health Research Initiative (jointly funded by CIHR, Israel Science Foundation, International Development Research Centre, Azrieli Foundation; IDRC 108875) to C.S., FCT grant PTDC/BIA-BID/29663/2017 to D.S.C., Intramural Research Program of the National Eye Institute, NIH (ZIAEY000450) to A. Swaroop, and Krembil Foundation and Canada First Research Excellence Fund/Medicine by Design to L. Attisano. C.S. holds the Dixon Family Chair in Ophthalmology Research, and J.B. holds the Calgary Firefighters Burn Treatment Society Chair in Skin Regeneration and Wound Healing. S.H. was supported by scholarships from the Cumming School of Medicine, Ontario Government Scholarship, UofT Vision Science Research Program, Peterborough K.M. HUNTER Charitable Foundation, and Margaret and Howard GAMBLE Research Grant; G.A.W. by Frederick Banting and Charles Best Canada, Alberta Innovates Health Solutions, and ACHRI/CIHR Training grant; S.O. by a FNR CORE grant (C15/BM/10397420); R.D. by a CIHR Canada HOPE Fellowship, and L. Adnani by an ACHRI/CIHR Training Grant.

AUTHOR CONTRIBUTIONS

Conceptualization, formal analysis, investigation, methodology, visualization, validation, writing – original draft, writing – review & editing, S.H. and G.A.W.; formal analysis, investigation, writing – review & editing, H.G., L. Adnani, R.D., L.T., I.F., V. Cortay, D.Z., A. Sivitilli, S.L., F.M., J.G., V. Chinchalongporn, A.-M.O., L.V., Y.T., L.A.D., E.R., J.-W.K., W.W., and W.R.; formal analysis, methodology, software, investigation, writing – review & editing, S.O., M.J.B., Y.I., and V.E.A.; validation, writing – original draft; writing – review & editing, J.A.C., I.K., L. Attisano, D.K., C.D., A. Swaroop, D.S.C., J.B., and A.d.S.; funding acquisition, conceptualization, project administration, resources, supervision, validation, writing – original draft; writing – review & editing, C.S.

DECLARATION OF INTERESTS

The authors declare no conflicts of interest.

Received: September 29, 2020
Revised: May 19, 2021
Accepted: July 8, 2021
Published: August 17, 2021

REFERENCES

Aydin, B., Kakumanu, A., Rossillo, M., Moreno-Estellés, M., Garipler, G., Ringstad, N., Flames, N., Mahony, S., and Mazzoni, E.O. (2019). Proneural factors Ascl1 and Neurog2 contribute to neuronal subtype identities by establishing distinct chromatin landscapes. Nat. Neurosci. *22*, 897–908.

Babicki, S., Arndt, D., Marcu, A., Liang, Y., Grant, J.R., Maciejewski, A., and Wishart, D.S. (2016). Heatmapper: web-enabled heat mapping for all. Nucleic Acids Res. *44* (W1), W147-53.

Ballas, N., Grunseich, C., Lu, D.D., Speh, J.C., and Mandel, G. (2005). REST and its corepressors mediate plasticity of neuronal gene chromatin throughout neurogenesis. Cell *121*, 645–657.

Beckervordersandforth, R., Tripathi, P., Ninkovic, J., Bayam, E., Lepier, A., Stempfhuber, B., Kirchhoff, F., Hirrlinger, J., Haslinger, A., Lie, D.C., et al. (2010). In vivo fate mapping and expression analysis reveals molecular hallmarks of prospectively isolated adult neural stem cells. Cell Stem Cell *7*, 744–758.

Betizeau, M., Cortay, V., Patti, D., Pfister, S., Gautier, E., Bellemin-Ménard, A., Afanassieff, M., Huissoud, C., Douglas, R.J., Kennedy, H., and Dehay, C. (2013). Precursor diversity and complexity of lineage relationships in the outer subventricular zone of the primate. Neuron *80*, 442–457.

Brand, M., and Morrissey, E. (2020). Single-cell fate decisions of bipotential hematopoietic progenitors. Curr. Opin. Hematol. *27*, 232–240.

Britz, O., Mattar, P., Nguyen, L., Langevin, L.M., Zimmer, C., Alam, S., Guillemot, F., and Schuurmans, C. (2006). A role for proneural genes in the maturation of cortical progenitor cells. Cereb. Cortex *16* (*Suppl 1*), i138–i151.

Buenrostro, J.D., Wu, B., Chang, H.Y., and Greenleaf, W.J. (2015). ATAC-seq: A Method for Assaying Chromatin Accessibility Genome-Wide. Curr. Protoc. Mol. Biol. *109*, 1–, 9.

Bunz, F., Dutriaux, A., Lengauer, C., Waldman, T., Zhou, S., Brown, J.P., Sedivy, J.M., Kinzler, K.W., and Vogelstein, B. (1998). Requirement for p53 and p21 to sustain G2 arrest after DNA damage. Science *282*, 1497–1501.

Butler, A., Hoffman, P., Smibert, P., Papalexi, E., and Satija, R. (2018). Integrating single-cell transcriptomic data across different conditions, technologies, and species. Nat. Biotechnol. *36*, 411–420.

Castro, D.S., Skowronska-Krawczyk, D., Armant, O., Donaldson, I.J., Parras, C., Hunt, C., Critchley, J.A., Nguyen, L., Gossler, A., Göttgens, B., et al. (2006). Proneural bHLH and Brn proteins coregulate a neurogenic program through cooperative binding to a conserved DNA motif. Dev. Cell *11*, 831–844.

Chaudhry, A.Z., Lyons, G.E., and Gronostajski, R.M. (1997). Expression patterns of the four nuclear factor I genes during mouse embryogenesis indicate a potential role in development. Dev. Dyn. *208*, 313–325.

Chou, S.J., and O'Leary, D.D. (2013). Role for Lhx2 in corticogenesis through regulation of progenitor differentiation. Mol. Cell. Neurosci. *56*, 1–9.

Coles-Takabe, B.L., Brain, I., Purpura, K.A., Karpowicz, P., Zandstra, P.W., Morshead, C.M., and van der Kooy, D. (2008). Don't look: growing clonal versus nonclonal neural stem cell colonies. Stem Cells *26*, 2938–2944.

Collombat, P., Mansouri, A., Hecksher-Sorensen, J., Serup, P., Krull, J., Gradwohl, G., and Gruss, P. (2003). Opposing actions of Arx and Pax4 in endocrine pancreas development. Genes Dev. *17*, 2591–2603.

Dalton, S. (2015). Linking the Cell Cycle to Cell Fate Decisions. Trends Cell Biol. *25*, 592–600.

de Juan Romero, C., Bruder, C., Tomasello, U., Sanz-Anquela, J.M., and Borrell, V. (2015). Discrete domains of gene expression in germinal layers distinguish the development of gyrencephaly. EMBO J. *34*, 1859–1874.

Del Toro, D., Ruff, T., Cederfjäll, E., Villalba, A., Seyit-Bremer, G., Borrell, V., and Klein, R. (2017). Regulation of Cerebral Cortex Folding by Controlling Neuronal Migration via FLRT Adhesion Molecules. Cell *169*, 621–635.e16.

Dennis, D.J., Wilkinson, G., Li, S., Dixit, R., Adnani, L., Balakrishnan, A., Han, S., Kovach, C., Gruenig, N., Kurrasch, D.M., et al. (2017). *Neurog2* and *Ascl1* together regulate a postmitotic derepression circuit to govern laminar fate specification in the murine neocortex. Proc. Natl. Acad. Sci. USA *114*, E4934–E4943.

Dillon, N. (2012). Factor mediated gene priming in pluripotent stem cells sets the stage for lineage specification. BioEssays *34*, 194–204.

Dixit, R., Zimmer, C., Waclaw, R.R., Mattar, P., Shaker, T., Kovach, C., Logan, C., Campbell, K., Guillemot, F., and Schuurmans, C. (2011). Ascl1 participates in Cajal-Retzius cell development in the neocortex. Cereb. Cortex *21*, 2599–2611.

Dixon, J.R., Jung, I., Selvaraj, S., Shen, Y., Antosiewicz-Bourget, J.E., Lee, A.Y., Ye, Z., Kim, A., Rajagopal, N., Xie, W., et al. (2015). Chromatin architecture reorganization during stem cell differentiation. Nature *518*, 331–336.

Dray, N., Mancini, L., Binshtok, U., Cheysson, F., Supatto, W., Mahou, P., Bedu, S., Ortica, S., Than-Trong, E., Krecsmarik, M., et al. (2021). Dynamic spatiotemporal coordination of neural stem cell fate decisions occurs through local feedback in the adult vertebrate brain. Cell Stem Cell. Published online April 2, 2021. https://doi.org/10.1016/j.stem.2021.03.014.

Fiddes, I.T., Lodewijk, G.A., Mooring, M., Bosworth, C.M., Ewing, A.D., Mantalas, G.L., Novak, A.M., van den Bout, A., Bishara, A., Rosenkrantz, J.L., et al. (2018). Human-Specific NOTCH2NL Genes Affect Notch Signaling and Cortical Neurogenesis. Cell *173*, 1356–1369.e22.

Fode, C., Gradwohl, G., Morin, X., Dierich, A., LeMeur, M., Goridis, C., and Guillemot, F. (1998). The bHLH protein NEUROGENIN 2 is a determination factor for epibranchial placode-derived sensory neurons. Neuron *20*, 483–494.

Furutachi, S., Miya, H., Watanabe, T., Kawai, H., Yamasaki, N., Harada, Y., Imayoshi, I., Nelson, M., Nakayama, K.I., Hirabayashi, Y., and Gotoh, Y. (2015). Slowly dividing neural progenitors are an embryonic origin of adult neural stem cells. Nat. Neurosci. *18*, 657–665.

Gradwohl, G., Fode, C., and Guillemot, F. (1996). Restricted expression of a novel murine atonal-related bHLH protein in undifferentiated neural precursors. Dev. Biol. *180*, 227–241.

Graf, T., and Enver, T. (2009). Forcing cells to change lineages. Nature *462*, 587–594.

Hagey, D.W., Zaouter, C., Combeau, G., Lendahl, M.A., Andersson, O., Huss, M., and Muhr, J. (2016). Distinct transcription factor complexes act on a permissive chromatin landscape to establish regionalized gene expression in CNS stem cells. Genome Res. *26*, 908–917.

Han, S., Dennis, D.J., Balakrishnan, A., Dixit, R., Britz, O., Zinyk, D., Touahri, Y., Olender, T., Brand, M., Guillemot, F., et al. (2018). A non-canonical role for the proneural gene *Neurog1* as a negative regulator of neocortical neurogenesis. Development *145*, 145.

Heinz, S., Benner, C., Spann, N., Bertolino, E., Lin, Y.C., Laslo, P., Cheng, J.X., Murre, C., Singh, H., and Glass, C.K. (2010). Simple combinations of lineage-determining transcription factors prime cis-regulatory elements required for macrophage and B cell identities. Mol. Cell *38*, 576–589.

Heng, J.I., Nguyen, L., Castro, D.S., Zimmer, C., Wildner, H., Armant, O., Skowronska-Krawczyk, D., Bedogni, F., Matter, J.M., Hevner, R., and Guillemot, F. (2008). Neurogenin 2 controls cortical neuron migration through regulation of Rnd2. Nature *455*, 114–118.

Hirrlinger, J., Scheller, A., Hirrlinger, P.G., Kellert, B., Tang, W., Wehr, M.C., Goebbels, S., Reichenbach, A., Sprengel, R., Rossner, M.J., and Kirchhoff, F. (2009). Split-cre complementation indicates coincident activity of different genes in vivo. PLoS ONE *4*, e4286.

Huang, H.P., Liu, M., El-Hodiri, H.M., Chu, K., Jamrich, M., and Tsai, M.J. (2000). Regulation of the pancreatic islet-specific gene BETA2 (neuroD) by neurogenin 3. Mol. Cell. Biol. *20*, 3292–3307.

John, S., Sabo, P.J., Thurman, R.E., Sung, M.H., Biddie, S.C., Johnson, T.A., Hager, G.L., and Stamatoyannopoulos, J.A. (2011). Chromatin accessibility pre-determines glucocorticoid receptor binding patterns. Nat. Genet. *43*, 264–268.

Kippin, T.E., Martens, D.J., and van der Kooy, D. (2005). p21 loss compromises the relative quiescence of forebrain stem cell proliferation leading to exhaustion of their proliferation capacity. Genes Dev. *19*, 756–767.

Kriegstein, A., Noctor, S., and Martínez-Cerdeño, V. (2006). Patterns of neural stem and progenitor cell division may underlie evolutionary cortical expansion. Nat. Rev. Neurosci. *7*, 883–890.

Kuleshov, M.V., Jones, M.R., Rouillard, A.D., Fernandez, N.F., Duan, Q., Wang, Z., Koplev, S., Jenkins, S.L., Jagodnik, K.M., Lachmann, A., et al. (2016). Enrichr: a comprehensive gene set enrichment analysis web server 2016 update. Nucleic Acids Res. *44* (W1), W90-7.

Lagha, M., Brunelli, S., Messina, G., Cumano, A., Kume, T., Relaix, F., and Buckingham, M.E. (2009). Pax3:Foxc2 reciprocal repression in the somite

modulates muscular versus vascular cell fate choice in multipotent progenitors. Dev. Cell *17*, 892–899.

Leung, C.T., Coulombe, P.A., and Reed, R.R. (2007). Contribution of olfactory neural stem cells to tissue maintenance and regeneration. Nat. Neurosci. *10*, 720–726.

Lewitus, E., Kelava, I., and Huttner, W.B. (2013). Conical expansion of the outer subventricular zone and the role of neocortical folding in evolution and development. Front. Hum. Neurosci. *7*, 424.

Lewitus, E., Kelava, I., Kalinka, A.T., Tomancak, P., and Huttner, W.B. (2014). An adaptive threshold in mammalian neocortical evolution. PLoS Biol. *12*, e1002000.

Li, H., and Durbin, R. (2009). Fast and accurate short read alignment with Burrows-Wheeler transform. Bioinformatics *25*, 1754–1760.

Li, H., Handsaker, B., Wysoker, A., Fennell, T., Ruan, J., Homer, N., Marth, G., Abecasis, G., and Durbin, R.; 1000 Genome Project Data Processing Subgroup (2009). The Sequence Alignment/Map format and SAMtools. Bioinformatics *25*, 2078–2079.

Li, S., Mattar, P., Zinyk, D., Singh, K., Chaturvedi, C.P., Kovach, C., Dixit, R., Kurrasch, D.M., Ma, Y.C., Chan, J.A., et al. (2012). GSK3 temporally regulates neurogenin 2 proneural activity in the neocortex. J. Neurosci. *32*, 7791–7805.

Li, S., Mattar, P., Dixit, R., Lawn, S.O., Wilkinson, G., Kinch, C., Eisenstat, D., Kurrasch, D.M., Chan, J.A., and Schuurmans, C. (2014). RAS/ERK signaling controls proneural genetic programs in cortical development and gliomagenesis. J. Neurosci. *34*, 2169–2190.

Llinares-Benadero, C., and Borrell, V. (2019). Deconstructing cortical folding: genetic, cellular and mechanical determinants. Nat. Rev. Neurosci. *20*, 161–176.

Love, M.I., Huber, W., and Anders, S. (2014). Moderated estimation of fold change and dispersion for RNA-seq data with DESeq2. Genome Biol. *15*, 550.

Lukaszewicz, A., Savatier, P., Cortay, V., Giroud, P., Huissoud, C., Berland, M., Kennedy, H., and Dehay, C. (2005). G1 phase regulation, area-specific cell cycle control, and cytoarchitectonics in the primate cortex. Neuron *47*, 353–364.

Ma, Y., Kanakousaki, K., and Buttitta, L. (2015). How the cell cycle impacts chromatin architecture and influences cell fate. Front. Genet. *6*, 19.

Martínez-Martínez, M.A., De Juan Romero, C., Fernández, V., Cárdenas, A., Götz, M., and Borrell, V. (2016). A restricted period for formation of outer subventricular zone defined by Cdh1 and Trnp1 levels. Nat. Commun. *7*, 11812.

Masserdotti, G., Gillotin, S., Sutor, B., Drechsel, D., Irmler, M., Jørgensen, H.F., Sass, S., Theis, F.J., Beckers, J., Berninger, B., et al. (2015). Transcriptional Mechanisms of Proneural Factors and REST in Regulating Neuronal Reprogramming of Astrocytes. Cell Stem Cell *17*, 74–88.

Matsumoto, N., Shinmyo, Y., Ichikawa, Y., and Kawasaki, H. (2017). Gyrification of the cerebral cortex requires FGF signaling in the mammalian brain. eLife *6*, 6.

Mattar, P., Langevin, L.M., Markham, K., Klenin, N., Shivji, S., Zinyk, D., and Schuurmans, C. (2008). Basic helix-loop-helix transcription factors cooperate to specify a cortical projection neuron identity. Mol. Cell. Biol. *28*, 1456–1469.

McQuin, C., Goodman, A., Chernyshev, V., Kamentsky, L., Cimini, B.A., Karhohs, K.W., Doan, M., Ding, L., Rafelski, S.M., Thirstrup, D., et al. (2018). CellProfiler 3.0: Next-generation image processing for biology. PLoS Biol. *16*, e2005970.

Miyata, T., Kawaguchi, A., Saito, K., Kawano, M., Muto, T., and Ogawa, M. (2004). Asymmetric production of surface-dividing and non-surface-dividing cortical progenitor cells. Development *131*, 3133–3145.

Nonaka-Kinoshita, M., Reillo, I., Artegiani, B., Martínez-Martínez, M.A., Nelson, M., Borrell, V., and Calegari, F. (2013). Regulation of cerebral cortex size and folding by expansion of basal progenitors. EMBO J. *32*, 1817–1828.

Nowakowski. (2016). Transformation of the Radial Glia Scaffold Demarcates Two Stages of Human Cerebral Cortex Development. Neuron.

Okawa, S., Angarica, V.E., Lemischka, I., Moore, K., and Del Sol, A. (2015). A differential network analysis approach for lineage specifier prediction in stem cell subpopulations. NPJ Syst. Biol. Appl. *1*, 15012.

Okawa, S., Nicklas, S., Zickenrott, S., Schwamborn, J.C., and Del Sol, A. (2016). A Generalized Gene-Regulatory Network Model of Stem Cell Differentiation for Predicting Lineage Specifiers. Stem Cell Reports *7*, 307–315.

Oproescu, A.M., Han, S., and Schuurmans, C. (2021). New Insights Into the Intricacies of Proneural Gene Regulation in the Embryonic and Adult Cerebral Cortex. Front. Mol. Neurosci. *14*, 642016.

Ottone, C., Krusche, B., Whitby, A., Clements, M., Quadrato, G., Pitulescu, M.E., Adams, R.H., and Parrinello, S. (2014). Direct cell-cell contact with the vascular niche maintains quiescent neural stem cells. Nat. Cell Biol. *16*, 1045–1056.

Palii, C.G., Cheng, Q., Gillespie, M.A., Shannon, P., Mazurczyk, M., Napolitani, G., Price, N.D., Ranish, J.A., Morrissey, E., Higgs, D.R., and Brand, M. (2019). Single-Cell Proteomics Reveal that Quantitative Changes in Co-expressed Lineage-Specific Transcription Factors Determine Cell Fate. Cell Stem Cell *24*, 812–820.e5.

Parras, C.M., Schuurmans, C., Scardigli, R., Kim, J., Anderson, D.J., and Guillemot, F. (2002). Divergent functions of the proneural genes Mash1 and Ngn2 in the specification of neuronal subtype identity. Genes Dev. *16*, 324–338.

Parras, C.M., Hunt, C., Sugimori, M., Nakafuku, M., Rowitch, D., and Guillemot, F. (2007). The proneural gene Mash1 specifies an early population of telencephalic oligodendrocytes. J. Neurosci. *27*, 4233–4242.

Peukert, D., Weber, S., Lumsden, A., and Scholpp, S. (2011). Lhx2 and Lhx9 determine neuronal differentiation and compartition in the caudal forebrain by regulating Wnt signaling. PLoS Biol. *9*, e1001218.

Piper, J., Elze, M.C., Cauchy, P., Cockerill, P.N., Bonifer, C., and Ott, S. (2013). Wellington: a novel method for the accurate identification of digital genomic footprints from DNase-seq data. Nucleic Acids Res. *41*, e201.

Plummer, N.W., Ungewitter, E.K., Smith, K.G., Yao, H.H., and Jensen, P. (2017). A new mouse line for cell ablation by diphtheria toxin subunit A controlled by a Cre-dependent FLEx switch. Genesis *55*, 55.

Ponti, G., Obernier, K., Guinto, C., Jose, L., Bonfanti, L., and Alvarez-Buylla, A. (2013). Cell cycle and lineage progression of neural progenitors in the ventricular-subventricular zones of adult mice. Proc. Natl. Acad. Sci. USA *110*, E1045–E1054.

Qiu, X., Mao, Q., Tang, Y., Wang, L., Chawla, R., Pliner, H.A., and Trapnell, C. (2017). Reversed graph embedding resolves complex single-cell trajectories. Nat. Methods *14*, 979–982.

Raposo, A.A.S.F., Vasconcelos, F.F., Drechsel, D., Marie, C., Johnston, C., Dolle, D., Bithell, A., Gillotin, S., van den Berg, D.L.C., Ettwiller, L., et al. (2015). Ascl1 Coordinately Regulates Gene Expression and the Chromatin Landscape during Neurogenesis. Cell Rep. *10*, 1544–1556.

Rash, B.G., Tomasi, S., Lim, H.D., Suh, C.Y., and Vaccarino, F.M. (2013). Cortical gyrification induced by fibroblast growth factor 2 in the mouse brain. J. Neurosci. *33*, 10802–10814.

Reillo, I., de Juan Romero, C., García-Cabezas, M.A., and Borrell, V. (2011). A role for intermediate radial glia in the tangential expansion of the mammalian cerebral cortex. Cereb. Cortex *21*, 1674–1694.

Robinson, M.D., McCarthy, D.J., and Smyth, G.K. (2010). edgeR: a Bioconductor package for differential expression analysis of digital gene expression data. Bioinformatics *26*, 139–140.

Rosin, J.M., Marsters, C.M., Malik, F., Far, R., Adnani, L., Schuurmans, C., Pittman, Q.J., and Kurrasch, D.M. (2021). Embryonic Microglia Interact with Hypothalamic Radial Glia during Development and Upregulate the TAM Receptors MERTK and AXL following an Insult. Cell Rep. *34*, 108587.

Ross-Innes, C.S., Stark, R., Teschendorff, A.E., Holmes, K.A., Ali, H.R., Dunning, M.J., Brown, G.D., Gojis, O., Ellis, I.O., Green, A.R., et al. (2012). Differential oestrogen receptor binding is associated with clinical outcome in breast cancer. Nature *481*, 389–393.

Schindelin, J., Arganda-Carreras, I., Frise, E., Kaynig, V., Longair, M., Pietzsch, T., Preibisch, S., Rueden, C., Saalfeld, S., Schmid, B., et al. (2012). Fiji: an open-source platform for biological-image analysis. Nat. Methods *9*, 676–682.

Sessa, A., Ciabatti, E., Drechsel, D., Massimino, L., Colasante, G., Giannelli, S., Satoh, T., Akira, S., Guillemot, F., and Broccoli, V. (2017). The Tbr2 Molecular Network Controls Cortical Neuronal Differentiation Through Complementary Genetic and Epigenetic Pathways. Cereb. Cortex *27*, 3378–3396.

Shannon, P., Markiel, A., Ozier, O., Baliga, N.S., Wang, J.T., Ramage, D., Amin, N., Schwikowski, B., and Ideker, T. (2003). Cytoscape: a software environment for integrated models of biomolecular interaction networks. Genome Res. *13*, 2498–2504.

Shen, L., Shao, N., Liu, X., and Nestler, E. (2014). ngs.plot: Quick mining and visualization of next-generation sequencing data by integrating genomic databases. BMC Genomics *15*, 284.

Sivitilli, A.A., Gosio, J.T., Ghoshal, B., Evstratova, A., Trcka, D., Ghiasi, P., Hernandez, J.J., Beaulieu, J.M., Wrana, J.L., and Attisano, L. (2020). Robust production of uniform human cerebral organoids from pluripotent stem cells. Life Sci Alliance *3*, e202000707.

Stahl, R., Walcher, T., De Juan Romero, C., Pilz, G.A., Cappello, S., Irmler, M., Sanz-Aquela, J.M., Beckers, J., Blum, R., Borrell, V., and Götz, M. (2013). Trnp1 regulates expansion and folding of the mammalian cerebral cortex by control of radial glial fate. Cell *153*, 535–549.

Stergachis, A.B., Neph, S., Reynolds, A., Humbert, R., Miller, B., Paige, S.L., Vernot, B., Cheng, J.B., Thurman, R.E., Sandstrom, R., et al. (2013). Developmental fate and cellular maturity encoded in human regulatory DNA landscapes. Cell *154*, 888–903.

Sutcu, H.H., and Ricchetti, M. (2018). Loss of heterogeneity, quiescence, and differentiation in muscle stem cells. Stem Cell Investig. *5*, 9.

Talos, F., Abraham, A., Vaseva, A.V., Holembowski, L., Tsirka, S.E., Scheel, A., Bode, D., Dobbelstein, M., Brück, W., and Moll, U.M. (2010). p73 is an essential regulator of neural stem cell maintenance in embryonal and adult CNS neurogenesis. Cell Death Differ. *17*, 1816–1829.

Telley, L., Agirman, G., Prados, J., Amberg, N., Fièvre, S., Oberst, P., Bartolini, G., Vitali, I., Cadilhac, C., Hippenmeyer, S., et al. (2019). Temporal patterning of apical progenitors and their daughter neurons in the developing neocortex. Science *364*, 364.

Wang, X., Tsai, J.W., LaMonica, B., and Kriegstein, A.R. (2011). A new subtype of progenitor cell in the mouse embryonic neocortex. Nat. Neurosci. *14*, 555–561.

Wapinski, O.L., Vierbuchen, T., Qu, K., Lee, Q.Y., Chanda, S., Fuentes, D.R., Giresi, P.G., Ng, Y.H., Marro, S., Neff, N.F., et al. (2013). Hierarchical mechanisms for direct reprogramming of fibroblasts to neurons. Cell *155*, 621–635.

Weber-Adrian, D., Kofoed, R.H., Silburt, J., Noroozian, Z., Shah, K., Burgess, A., Rideout, S., Kügler, S., Hynynen, K., and Aubert, I. (2021). Systemic AAV6-synapsin-GFP administration results in lower liver biodistribution, compared to AAV1&2 and AAV9, with neuronal expression following ultrasound-mediated brain delivery. Sci. Rep. *11*, 1934.

Zhong, S., Zhang, S., Fan, X., Wu, Q., Yan, L., Dong, J., Zhang, H., Li, L., Sun, L., Pan, N., et al. (2018). A single-cell RNA-seq survey of the developmental landscape of the human prefrontal cortex. Nature *555*, 524–528.

Please cite this article in press as: Han et al., Proneural genes define ground-state rules to regulate neurogenic patterning and cortical folding, Neuron (2021), https://doi.org/10.1016/j.neuron.2021.07.007

STAR★METHODS

KEY RESOURCES TABLE

REAGENT or RESOURCE	SOURCE	IDENTIFIER
Antibodies		
Goat anti-Neurogenin2	Santacruz	Cat# sc-19231; RRID: AB_2298242
Rabbit anti-Neurogenin2	Invitrogen	Cat# PA5-78556; RRID: AB_2736211
Mouse anti-Ascl1(Clone 24B72D11.1)	BD PharMingen	Cat# 556604; RRID: AB_396479
Goat anti-GFP	Abcam	Cat# ab5450; RRID: AB_304897
Rabbit anti-GFP	Molecular Probes	Cat# A-11122; RRID: AB_221569
Goat anti-mCherry (also used for tdTomato detection)	Sicgen	Cat# AB0040; RRID: AB_10993324
Rat anti-mCherry	Invitrogen	Cat# M11217; RRID: AB_2536611
Rabbit anti-NeuN	Abcam	Cat# ab177487; RRID: AB_2298772
Mouse anti-NeuN (Clone A60)	Millipore	Cat# MAB377; RRID: AB_2298772
Rabbit anti-Ki67	Abcam	Cat# ab16667; RRID: AB_302459
Rat anti-BrdU (Clone BU1/75 (ICR1))	Thermofisher	Cat# MA1-82088; RRID: AB_927214
Mouse anti-BrdU (Clone MoBU-1)	Thermofisher	Cat# B35128; RRID: AB_2536432
Alexa Fluor 647 Mouse Anti-SSEA-1 (Clone MC480)	BD Bioscience	Cat# 560120; RRID: AB_11151898
APC Rat anti-CD133 (Prominin-1) (Clone 13A4)	eBioscience	Cat# 17-1331-81; RRID: AB_823120
PerCP-eFluor 710 Rat anti-CD133 (Prominin-1) (Clone 13A4)	eBioscience	Cat# 46-1331-82; RRID: AB_10670743
Mouse anti-β3-tubulin (Clone TUBB3)	BioLegend	Cat# 801202; RRID: AB_10063408
Goat anti-Pdgfrα	R&D Systems	Cat# AF1062; RRID: AB_2236897
Rat anti-Pdgfrα (Clone APA5)	BD PharMingen	Cat# 558774; RRID: AB_397117
Rabbit anti-GFAP	DakoCytomation	Cat# Z0334; RRID: AB_10013382
Rat anti-GFAP (Clone 2.2B10)	Thermofisher	Cat# 13-0300; RRID: AB_2532994
Rabbit anti-Sox9	Millipore	Cat# AB5535; RRID: AB_2239761
Rabbit anti-Pax6	Convance	Cat# PRB-278P; RRID: AB_291612
Rabbit anti-Tbr2	Abcam	Cat# ab23345; RRID: AB_778267
Rabbit anti-zsGreen	Takara	Cat# 632474; RRID: AB_2491179
Rabbit anti-Tbr1	Abcam	Cat# ab31940; RRID: AB_2200219
Mouse anti-Satb2 (clone SATBA4B10)	Abcam	Cat# ab51502; RRID: AB_882455
Rabbit anti-Blbp	Abcam	Cat# ab32423; RRID: AB_880078
Rabbit anti-Laminin	Sigma	Cat# ab32423; RRID: AB_477163
Anti-FLAG M1 Agarose Affinity Gel	Sigma	Cat# L9393; RRID: AB_10062709
Rabbit anti-FLAG	Cell Signaling	Cat# 2368; RRID: AB_2217020
Rabbit anti-GAPDH (Clone 14C10)	Cell Signaling	Cat# 2118; RRID: AB_561053
Rabbit anti-Notch (Cleaved) (NICD)	Cell Signaling	Cat# 4147; RRID: AB_2153348
Rabbit anti-S100b	Dako/Agilent	Cat# Z031129-2; RRID: AB_2315306
Rabbit anti-phospho-histone H3 (pHH3)	Millipore	Cat# 06-570; RRID: AB_310177
Rabbit anti-Nfia	Sigma-Aldrich	Cat# HPA006111; RRID: AB_1854422
Rabbit anti-Bhlhe22	Sigma-Aldrich	Cat# HPA064872; RRID: AB_2685377
Chemicals, peptides, and recombinant proteins		
Opal 690 reagent	Akoya	Cat# FP1497001KT
Opal 570 reagent	Akoya	Cat# FP1488001KT
Opal 520 reagent	Akoya	Cat# FP1487001KT

(*Continued on next page*)

Please cite this article in press as: Han et al., Proneural genes define ground-state rules to regulate neurogenic patterning and cortical folding, Neuron (2021), https://doi.org/10.1016/j.neuron.2021.07.007

Continued

REAGENT or RESOURCE	SOURCE	IDENTIFIER
Viability Dye eFluor 780	eBioscience	Cat# 65-0865-14
Hoechst 33342	Thermofisher	Cat# 62249
B27 supplement minus vitamin A	Thermofisher	Cat# 12587010
Human FGF2	MACS	Cat# 130-093-842
Animal-Free Recombinant Human EGF	Peprotech	Cat# AF-100-15
Cyclopamine	Selleckchem	Cat# S1146
Geltrex matrix	Thermofisher	Cat# 12760
StemProNeural Supplement	Thermofisher	Cat# A1050801
B27 supplement	Thermofisher	Cat# 17504
N-2 Supplement	Thermofisher	Cat# 17502
T3 (3,3′,5-Triiodo-L-thyronine sodium salt)	Sigma	Cat# D6397
DNaseI	Ambion	Cat# AM2222
Critical commercial assays		
RNAscope Multiplex Fluorescent Detection Kit v2	ACD	Cat# 323110
Dual-Luciferase Reporter Assay System	Promega	Cat# E1910
Nucleofector Kits for Mouse Neural Stem Cells (mNSC)	Lonza	Cat# VPG-1004
Duolink *In Situ* Red Starter Kit Goat/Rabbit	Sigma Aldrich	Cat# DUO92105
MagMAX-96 Total RNA Isolation Kit	Invitrogen	Cat# AM1830
TruSeq Stranded mRNA Library Prep Kit	Illumina	Cat# 15028212
RNeasy Micro Kit	QIAGEN	Cat# 74004
RT^2 First strand kit	QIAGEN	Cat# 330401
RT^2 SYBR Green qPCR Mastermix	QIAGEN	Cat# 330500
QX200 droplet digital PCR (ddPCR) system, and ddPCR Supermix	Bio-Rad	Cat# 1864001, Cat#1863023
Click-iT Plus EdU Imaging Kit (Alexa Fluor 647 dye)	Invitrogen	Cat# C10640
Click-iT Plus TUNEL Assay kit (Alexa Fluor 647 dye)	Invitrogen	Cat# C10619
Deposited data		
RNA-seq data	This study	GEO: GSE151775
ATAC-seq data	This study	GEO: GSE84120
Ascl1 ChIP-seq data	This study	Array Express: E-MTAB-9751 (https://www.ebi.ac.uk/arrayexpress/experiments/)
Neurog2 ChIP-seq data	Sessa et al., 2017	GEO: GSE63621
scRNA-seq data of human COs	Sivitilli et al., 2020	GEO: GSE137877
scRNA-seq data of human fetal cortex	Zhong et al., 2018)	GEO: GSE104276
Transcriptional interaction data	MetaCore (GeneGo Inc.)	https://portal.genego.com/
Uncropped western blot images	This study	Mendeley link: https://dx.doi.org/10.17632/wgpsd9yyk2.1
Experimental models: Cell lines		
P19 embryonic carcinoma cells	ATCC	CRL-1825; RRID: CVCL_2153
NIH 3T3 cells	ATCC	CRL-1658; RRID: CVCL_0594
Feeder-free H1 hESCs	Wicell	WA01; RRID: CVCL_9771
Experimental models: Organisms/strains		
Mus musculus: CD1 mouse (022)	Charles River	Strain Code: 022; RRID: IMSR_CRL:022
Mus musculus: *Neurog2*^{mCherryKI}	This study	N/A
Mus musculus: *Ascl1*^{GFPKI}	Leung et al., 2007	Jackson Laboratory Cat# 012881; RRID: IMSR_JAX:012881
Mus musculus: C57BL/6J	Jackson Laboratory	Cat# 000664; RRID: IMSR_JAX:000664
Mus musculus: Neurog2$^{N\text{-}CreKI}$	This study	N/A

(*Continued on next page*)

Please cite this article in press as: Han et al., Proneural genes define ground-state rules to regulate neurogenic patterning and cortical folding, Neuron (2021), https://doi.org/10.1016/j.neuron.2021.07.007

Continued

REAGENT or RESOURCE	SOURCE	IDENTIFIER
Mus musculus: Ascl1$^{C\text{-}CreKI}$	This study	N/A
Mus musculus: ROSA-tdTomato	Jackson Laboratory	Cat# 007905; RRID: IMSR_JAX:007905
Mus musculus: ROSA-zsGreen	Jackson Laboratory	Cat# 007906; RRID: IMSR_JAX:007906
Mus musculus: ROSA-DTA	Jackson Laboratory	Cat# 009669; RRID: IMSR_JAX:009669
Mus musculus: ROSA-DTR	Jackson Laboratory	Cat# 007900; RRID: IMSR_JAX:007900
Mus musculus: RC::L-DTA	Jackson Laboratory	Cat# 026944; RRID: IMSR_JAX:026944
Cynomolgus monkey (*Macaca fascicularis*)	Lukaszewicz et al., 2005	N/A
Oligonucleotides		
qPCR primers, see Table S6	QIAGEN	N/A
RNAscope probes, see Table S6	ACD	N/A
Genotyping primers, see Table S6	This study	N/A
ddPCR primers and probes, see Table S6	This study	N/A
Recombinant DNA		
p*NeuroD*^{1kb}	Huang et al., 2000	N/A
p*Rnd2*	Heng et al., 2008	N/A
p*Dll1M*	Castro et al., 2006	N/A
p*Dll1*	Castro et al., 2006	N/A
pCS108-FLAG	Han et al., 2018	N/A
pCS108-*Neurog2*-FLAG	Han et al., 2018	N/A
pCIG2-*Neurog2*	Mattar et al., 2008	N/A
pCIG2-*Ascl1*	Dixit et al., 2011	N/A
pCIG2-*Neurog2~Neurog2*	Li et al., 2012	N/A
pCIG2-*Neurog2~Ascl1*	This study	N/A
Nfia riboprobe template	Chaudhry et al., 1997	N/A
Zfp423 riboprobe template	Horizon Discovery	MMM1013-202732110
Klf13 riboprobe template	Source Bioscience	F630217D22
Foxp4 riboprobe template	Horizon Discovery	MMM1013-202859017
Software and algorithms		
Fiji (ImageJ)	Schindelin et al., 2012	https://imagej.net/software/fiji
CellProfiler	McQuin et al., 2018	https://cellprofiler.org/; RRID: SCR_007358
GraphPad Prism	GraphPad Software	https://www.graphpad.com/; RRID: SCR_002798
Cytoscape	Shannon et al., 2003	https://cytoscape.org/; RRID: SCR_003032
Burrows-Wheeler Aligner 0.7.12 (bwa mem)	Li and Durbin, 2009	http://bio-bwa.sourceforge.net/; RRID: SCR_010910
Samtools 1.9	Li et al., 2009	http://samtools.sourceforge.net/; RRID: SCR_005227
DESeq2	Love et al., 2014	https://bioconductor.org/packages/release/bioc/html/DESeq2.html; RRID: SCR_015687
NGSPLOT	Shen et al., 2014	https://github.com/shenlab-sinai/ngsplot; RRID: SCR_011795
Hotspot v.4	John et al., 2011	https://www.encodeproject.org/software/hotspot/
Diffbind	Ross-Innes et al., 2012	http://bioconductor.org/packages/release/bioc/html/DiffBind.html; RRID: SCR_012918
Gene Ontology	https://doi.org/10.1093/nar/gku1179	http://geneontology.org/; RRID: SCR_002811
EnrichR	Kuleshov et al., 2016	https://maayanlab.cloud/Enrichr/; RRID: SCR_001575
Heatmapper	Babicki et al., 2016	http://heatmapper.ca/; RRID: SCR_016974

(*Continued on next page*)

Please cite this article in press as: Han et al., Proneural genes define ground-state rules to regulate neurogenic patterning and cortical folding, Neuron (2021), https://doi.org/10.1016/j.neuron.2021.07.007

Continued

REAGENT or RESOURCE	SOURCE	IDENTIFIER
Biobase TRANSFAC	https://doi.org/10.1093/nar/gkj143	http://genexplain.com/transfac/; RRID: SCR_005620
Homer	Heinz et al., 2010	http://homer.ucsd.edu/homer/; RRID: SCR_010881
Gene regulatory network (GRN)	Okawa et al., 2015	https://www.nature.com/articles/npjsba201512
in silico perturbation assay	Okawa et al., 2015	https://www.nature.com/articles/npjsba201512
Seurat v.3.2.3	Butler et al., 2018	http://satijalab.org/seurat
Monocle3	Qiu et al., 2017	http://cole-trapnell-lab.github.io/monocle-release

RESOURCE AVAILABILITY

Lead Contact

Further information and request for resources and reagents should be directed to and will be fulfilled by the Lead Contact, Carol Schuurmans (cschuurm@sri.utoronto.ca).

Materials Availability

Plasmids generated in this study will be available upon request. Transgenic mouse lines generated in this study are not deposited in a central repository. As we are limited in the number of stock animals that we can maintain, the transfer of animals is possible only with reasonable compensation for processing and shipping and a completed Materials Transfer Agreement if there is a potential for commercial application.

Data and Code Availability

- RNA-seq and ATAC-seq data were deposited at GEO, ChIP-seq data was deposited at Array Express, and uncropped western blot images were deposited in Mendeley data at Mendeley. Accession numbers are listed in the Key Resources Table. These data are publicly available as of the date of publication. All other data reported in this study will be shared by the lead contact upon request.
- This paper does not report original code.
- Any additional information required to reanalyze the data reported in this work paper is available from the Lead Contact upon request.

EXPERIMENTAL MODELS AND SUBJECT DETAILS

None of our experimental animals had been previously used for other procedures. All animals were healthy.

Mice

Animal sources and maintenance

Embryos and pups were used between embryonic day (E)12.5-E18.5 and postnatal day (P) 0-P21, as outlined in the text and figures. Animal procedures were approved by the University of Calgary Animal Care Committee (AC11-0053) and later by the Sunnybrook Research Institute (16-606) in compliance with the Guidelines of the Canadian Council of Animal Care. The generation of *Ascl1*^{GFPKI} (Leung et al., 2007) (Jackson Lab: 012881) and *Neurog2*^{GFPKI} (Britz et al., 2006) null mutant mice was previously described. Rosa-DTA (Jackson Lab: 009669), Rosa-DTR (Jackson Lab: 007900), RC::L-DTA (Jackson Lab: 026944), Rosa-tdTomato (Jackson Lab: 007909), and Rosa-zsGreen (Jackson Lab: 007906) mice were purchased from Jackson Laboratory. The generation of new transgenic mouse lines (*Neurog2*$^{Flag\text{-}mCherryKI}$, *Neurog2*$^{N\text{-}CreKI}$, *Ascl1*$^{C\text{-}CreKI}$) is described below. All animals were maintained on CD1 or C57Bl6 backgrounds, and wild-type littermates were used as controls. For timed pregnancies, the day of the vaginal plug was designated E0.5. Male and female embryos were pooled for all experiments as assigning sex at embryonic stages is not possible without prior PCR genotyping and cells/embryos must be used immediately post-dissection/dissociation. For transgenic studies, males and females were pooled to reduce animal usage due to the low frequency of acquiring double and triple transgenic animals.

Generation of transgenic mice

Neurog2$^{Flag\text{-}mCherryKI/+}$ mice were generated by homologous recombination in embryonic stem cells (ESCs) (Figure S1D). Briefly, we constructed a targeting vector (pPNT-Neurog2Flag-IRESmCherry-LPN) with long and short arms of *Neurog2* using our previous design (Fode et al., 1998; Parras et al., 2002), which was linearized by *Swa*I and electroporated in G4 (129xC57BL/6) ESCs. Transfected ESCs were isolated using positive-negative selection with G418/gancyclovir. Genomic DNA was digested with *Not*I/*Spe*I and probed with 5′ (1.5-kb *Not*I/*Kpn*I) and 3′ (1-kb *Eco*RI/*Spe*I) external probes by Southern blot (Fode et al., 1998). For wild-type DNA, the

Please cite this article in press as: Han et al., Proneural genes define ground-state rules to regulate neurogenic patterning and cortical folding, Neuron (2021), https://doi.org/10.1016/j.neuron.2021.07.007

5′ and 3′ probes recognized the same 18.3-kb fragment whereas, for mutant DNA, 8.3-kb 5′ and 11.6-kb 3′ fragments were recognized, respectively (Figure S1E). The U of Calgary Transgenic Services aggregated targeted cell lines with morulae to produce chimeras, which were bred with CD1 mice. Agouti offspring (germline transmission) were genotyped by PCR using primers *Neurog2Flag-mCherry**F and *Neurog2Flag-mCherry**R, which gave rise to a 413-bp mutant amplicon. 94°C/3 min plus 35 cycles of 94°C/1 min 55°C/1 min and 72°C/1 min using primers for wild-type (*Neurog2**F and *Neurog2**R) and 95°C/5 min plus 40 cycles of 95°C/1 min, 60°C/1 min and 72°C/1 min for mutant (*Neurog2Flag-mCherry**F and *Neurog2Flag-mCherry**R) alleles. *Neurog2**F: 5′ TAG ACG CAG TGA CTT CTG TGA CCG 3′. *Neurog2**R: 5′-ACC TCC TCT TCC TCC TTC AAC TCC-3′. *Neurog2Flag-mCherry**F: 5′-ACA AAC AAC GTC TGT AGC GAC CCT-3′. *Neurog2Flag-mCherry**R: 5′-CAC CTT GAA GCG CAT GAA CTC CTT-3′.

Neurog2$^{N\text{-}Cre\text{KI}}$ and *Ascl1*$^{C\text{-}Cre\text{KI}}$ transgenics were generated by Cyagen Biosciences (https://www.cyagen.com/us/en/) using homologous recombination in ESCs. Targeting strategies replaced genomic sequence between the *Neurog2* or *Ascl1* START and STOP codon with N-Cre (amino acids 19-59 in *Neurog2* locus) or C-Cre (amino acids 60-343 in *Ascl1* locus) modified with a nuclear-localization signal, GCN4 coiled-coil domain, flexible linker, and partial Cre-recombinase sequences (Beckervordersandforth et al., 2010; Hirrlinger et al., 2009), respectively. Targeting vectors were cloned by VectorBuilder (https://en.vectorbuilder.com) with 109-FUV-hGFAP-NCre or 106-FUV-P2-CCre, respectively.

Non-human primates

Animal sources and maintenance

The use of cynomolgus monkey (*Macaca fascicularis*) (Lukaszewicz et al., 2005) and all experimental protocols were approved by the Animal Care and Use Committee in Lyon (CELYNE; protocols C2EA42-12-11-0402-003 and APAFIS#3183). Surgical procedures and animal experimentation were in accordance with European requirements 2010/63/UE. Animals were housed in a controlled environment (temperature: 22 ± 1°C) with 12 h light/12 h dark cycle (lights on at 08:00 a.m.). All animals were given commercial monkey diet twice a day with tap water *ad libitum* and were fed fruits and vegetables once daily. During and after experiments, monkeys were under careful veterinary oversight to ensure good health. Foetuses from timed-pregnant cynomolgus monkeys (E73) were delivered by caesarean section as described (Lukaszewicz et al., 2005). Male or female fetuses were used indiscriminately to reduce animal number.

Human cerebral organoids

Generation of human cerebral organoids (COs)

Feeder-free H1 hESCs (WiCell) were cultured on Matrigel in TeSR-E8 kit for hESC/hiPSC maintenance (StemCell Tech; #05990). hESCs were used to generate COs using the STEMdiff Cerebral organoid Kit (StemCell Tech; #08570) and STEMdiff Cerebral Organoid Maturation Kit (StemCell Tech; #08571) as directed by the manufacturer. Culture of human ESCs received approval from the Canadian Institutes of Health Research (CIHR) Stem Cell Oversight Committee (SCOC) to CS and was approved by the Sunnybrook REB (PIN: 264-2018).

METHOD DETAILS

In utero electroporation

cDNA expression vectors were introduced into dorsal telencephalic (cortical) progenitors using *in utero* electroporation (Dixit et al., 2011; Li et al., 2012). pCIG2-*Neurog2* (Mattar et al., 2008) and pCIG2-*Ascl1* (Li et al., 2012) expression vectors were described previously. To generate a *Neurog2*∼*Ascl1* tethered construct, the following oligonucleotides were annealed to make a tether (as in (Li et al., 2012)), leaving *Pst*I ends for ligation: 5′-GGG GGT TCC GGC GGG GGT TCT GGA GGT GGG AGC GGC GGA GGG TCC GGC GGA GGA ACT GCA-3′; 5′GTT CCT CCG CCG GAC CCT CCG CCG CTC CCA CCT CCA GAA CCC CCG CCG GAA CCC CCT GCA-3′.

Injection of Diphtheria toxin

Diphtheria toxin (DT; Enzo Life Sciences Inc. BML-G135-0001) was injected IP at 25 ng/g body weight once per day from E12.5 to E17.5 into pregnant Rosa-DTR females crossed with a split-Cre male, followed by E18.5 dissection.

Sectioning and immunohistochemistry

Brains were dissected in phosphate-buffered saline (PBS) and fixed in 4% paraformaldehyde (PFA)/1X PBS overnight at 4°C. For cryosections, brains were washed three times in 1X PBS, cryoprotected in 20% sucrose/1X PBS overnight at 4°C, blocked in optical cutting temperature (OCT) compound, and cut at 10 μm on a Leica CM3050 cryostat. Immunohistochemistry was performed as described (Li et al., 2014). Briefly, prior to immunostaining, sections were blocked in 10% horse serum in 0.1% triton x-100 in PBS (PBST) for 1 h at room temperature. For vibratome sections, brains were dissected and post-fixed in 4% PFA for 48 h at 4°C, washed 3 times in 1X PBS and cut into 100 μm coronal sections using a Leica VT1000S vibratome. Floating sections were washed with 1X PBS, permeabilized with PBST, and blocked for 1 h in 10% heat-inactivated fetal bovine serum (FBS) in PBST. Primary antibodies included mouse anti-Ascl1 (1:100, BD Biosciences #556604), rabbit anti-Bhlhe22 (1:200, Sigma-Aldrich #HPA064872), rabbit anti-Blbp (1:500, Abcam #ab32423), rat anti-BrdU (1:50, BioRad #OBT0030S), mouse anti-BrdU (Mobu-1;

Please cite this article in press as: Han et al., Proneural genes define ground-state rules to regulate neurogenic patterning and cortical folding, Neuron (2021), https://doi.org/10.1016/j.neuron.2021.07.007

1:50, Invitrogen #B35128), rabbit anti-GFAP (1:500, DakoCytomation #Z0334), rat anti-GFAP antibody (1/500, Thermo Fisher Scientific #13-0300), rabbit anti-GFP (1:500, Invitrogen #A-11122), goat anti-GFP (1:500, Abcam #ab5449), chicken anti-GFP (1:500, Abcam#ab13970), rabbit anti-Ki67 (1:500, Abcam #16667), rabbit anti-Laminin (1:500, Sigma #L9393), rabbit anti-Neurog2 (1:500, Invitrogen #PA5-78556), goat anti-Neurog2 (1:500, Santa Cruz Biotechnology #sc-19233), goat anti-mCherry (also detects tdTomato; 1:500, Sicgen #AB0040), rat anti-mCherry (1:500, Invitrogen #M11217), rabbit anti-NeuN (1:500, Abcam #ab177487), mouse anti-NeuN (1:100, Chemicon #MAB377), rabbit anti-Nfia (1:100, Sigma-Aldrich #HPA0006111), rabbit anti-Pax6 (1:350, Cedarlane #PRB-278P), goat anti-Pdgfrα (1/500, R&D Systems #AF1062), rat anti-Pdgfrα (1:500, eBioscence #14-1401-82), rabbit anti-phospho-histone H3 (pHH3; 1:500; Millipore Biotechnology, 06-570), mouse anti-Satb2 (1:500, Abcam #ab51502), rabbit anti-S100b (1:100, Dako/Agilent #Z031129-2), rabbit anti-Sox9 (1:500, Millipore #AB5535), rabbit anti-Tbr1 (1:500, Abcam #Ab31940), rabbit anti-Tbr2 (1:500, Abcam #ab23345), mouse anti-Tuj1 (β3-tubulin, 1:500, BioLegend #801202) and rabbit anti-zsGreen (1:500, Takara #632474). Secondary antibodies were all diluted to 1/500 and conjugated to different fluorophores, including Cy3 (red: mouse IgG, Jackson Immunoresearch #715-166-150), Alexa Fluor 405 (blue: mouse IgG, Abcam #Ab175659), Alexa Fluor 488 (green: rabbit IgG #A21206; goat IgG #A11055; rat IgG #A21208; mouse IgG #A11029, mouse IgG1 #A21121; chicken IgG #A11039, all from Invitrogen), Alexa Fluor 568 (red: rabbit IgG #A10042; goat IgG #A11057; rat IgG #A11077; mouse IgG #A11004; mouse IgG1 #A21124) or Alexa Fluor 647 (far-red: rabbit IgG, Invitrogen #A31573; rat IgG, Jackson ImmunoResearch #712-605-153). After the immunostaining steps, brain sections were stained with DAPI (Invitrogen #D1306) and mounted using Aqua-Poly/Mount (Polysciences #18606).

BrdU staining and cell cycle analyses

Bromodeoxyuridine (BrdU; Sigma, Oakville, ON) was injected IP at 100 μg/g body weight 30 min or 24 h before dissection as indicated. To measure cell cycle length, BrdU were administered every 3 h up to 15 h in E12.5 pregnant dams. Mice cortices were dissected 30 min, 1, 2, 3, 6, 9 and 15 h after BrdU injection. For BrdU co-immunolabeling, sections were first immunolabeled with the other antibody (as indicated), post-fixed with 4% PFA for 10 min and washed 3 times in PBST. Sections were treated with 2N HCl for 25 min at 37°C, and immunolabeled with anti-BrdU.

RNA *in situ* hybridization

RNA *in situ* hybridization was performed as described (Li et al., 2012, 2014). The following templates were used to generate antisense riboprobes, with restriction enzyme and polymerase indicated: *Nfia* (*Kpn*I, T7) (Chaudhry et al., 1997), *Zfp423* (GenBank: BC079586, *Sal*I, T3), *Klf13* (GenBank: AK155298, *Sac*I, T3), *Foxp4* (GenBank: BC052407, *Sal*I, T3).

RNAscope assay

The RNAscope Multiplex Fluorescent Detection Kit v2 (ACD #323110) was used according to the manufacturer's directions. Briefly, cryosections were post-fixed with 4% PFA for 15 min at 4°C and then dehydrated in 50%, 70% and 100% EtOH for 5 min each at room temperature. Sections were incubated in H_2O_2 solution for 10 min at room temperature, in 1x target retrieval solution for 5 min at 95°C, and washed with distilled water. Protease Plus was added for 15 min at 40°C and removed with washing buffer. RNA probes were applied for 2 h at 40°C as indicated. Mouse probes included Mm-*Ascl1* (#313291), Mm-*Neurog2-C2* (#417291-C2), Mm-*Hes1* (#417701), and Mm-*Dll1-C3* (#425071-C3). Macaque probes included Mfa-*ASCL1* (#546591), Mmu-*HES1-C3* (#1032181-C3), Mmu-*HOPX-C3* (#885001-C3), Mfa-*NEUROG2*-C2 (#546581-C2) and Mmu-*PAX6-C3* (#884991-C3). Human probes included Hs-*ASCL1* (#459728) and Hs-*NEUROG2*-C2 (#546601-C2). Custom probes were designed to detect *N-Cre* (#1062701-C3) and *C-Cre* (#1058921-C2). Amplification and staining steps were performed according to manufacturer's instructions. Opal 520 (Akoya #FP1487001KT; 1:1500), Opal 570 (Akoya #FP1488001KT; 1:1500) and Opal 690 (Akyoya #FP1497001KT; 1:1500) were applied for staining channel 1, 2, or 3.

Time lapse imaging

Cortices from E14.5 *Neurog2*$^{Flag\text{-}mCherryKI}$;*Ascl1*$^{GFPKI/+}$ embryos were cut at 300 μm in ice cold DMEM/F12 using a Leica VT1200S vibratome. Time-lapse imaging was performed as described (Rosin et al., 2021). Briefly, cortical slices were immersed in ice cold type 1a collagen (Cellmatrix, Nitta Gelatin, cat. 631-00651) on 30 mm glass coverslips which were then incubated at 37°C in a Zeiss chamber system filled with 40% O_2, 5% CO_2, and 55% N_2. After a 30 min incubation, slices were cultured in 2-3 mL of slice culture medium as previously described (Rosin et al., 2021). Images were obtained on an inverted confocal microscope (Zeiss) with either a 20X or 40X objective. Pictures were taken every 10 min in ~20 μm Z stack sections with 8-10 images per stack. Using an automated platform, multiple regions on the same slice were imaged over an ~18 h period. Time lapse images were further processed and analyzed with Fiji (ImageJ) software (Schindelin et al., 2012).

Fluorescence activated cell sorting (FACS) and flow cytometry

E12.5 *Neurog2*$^{Flag\text{-}mcherryKI/+}$; *Ascl1*$^{GFPKI/+}$ cortices were dissected in PBS and then dissociated in PBS (Ca^{2+}/Mg^{2+} free) containing 25 μg/mL trypsin (Sigma #T1005-1G) for 10 min at 37°C. Digestion was stopped with 20% FBS and cells were triturated ~40 times. Cells were resuspended in PBS containing 5 mM EDTA and 0.1% BSA. Dissociated cells (2.5 μl/1 × 10^6 cells) were stained with Viability Dye eFluor 780 (eBioscience #65-0865-14) and with anti-CD15-Alexa Fluor 647 (BD Bioscience #560120) or

Please cite this article in press as: Han et al., Proneural genes define ground-state rules to regulate neurogenic patterning and cortical folding, Neuron (2021), https://doi.org/10.1016/j.neuron.2021.07.007

anti-CD133-APC (eBioscience #17-1331-81) and PerCP-eFluor 710 (eBioscience #46-1331-82) according to the manufacturer's directions. For cell cycle analysis, cells were also stained with Hoechst 33342 (Thermo Fisher Scientific #62249) according to the manufacturer's protocol. FACS and cell cycle analysis was performed with a BD FACS Aria III cell sorting system. Quantitation of cell cycle phases was performed with FlowJo software using a Dean Jett Fox algorithm.

Neurosphere assay

FACS sorted cells were seeded in 0.2% gelatin coated 24-well plates at clonal density (5,000 cells/well) and cultured for 7 days in Neurosphere media containing DMEM/F12 (3:1), human FGF2 (40 ng/mL), human EGF (20 ng/mL), B27 supplement minus vitamin A (2%), Penicillin/streptomycin (0.1%), Fungizone (40 ng/mL), and cyclopamine (0.5 μg/mL). After 7 days of culture, neurospheres were mechanically dissociated with ACCUTASE (Stem cell technology, Cat # 07922) and cultured as secondary neurospheres by seeding 5,000 cells into the wells of a 24 well plate and cultured for an additional seven days. Tertiary neurosphere assays were performed the same way, dissociating secondary neurospheres. Primary neurospheres were counted and photographed using an AxioVision program (Carl Zeiss).

Directed differentiation assay

FACS sorted cells were plated in 8 well chamber slides coated with poly-L-ornithine and laminin for the differentiation of neurons and oligodendrocytes, or Geltrex matrix (Thermo Fisher Scientific #12760) for the differentiation of astrocytes. Cells were incubated for 1 day in Stem cell media, containing KnockOut^{tm} D-MEM/F12, GlutaMax^{tm}-I supplement (2 mM), bFGF (20 ng/mL), EGF (20 ng/mL), 2% StemPro Neural Supplement, Penicillin/streptomycin (0.1%) and Antibiotic-Antimycotic solution (1%). To induce neuronal differentiation, cells were grown in Neurobasal medium, 2% B-27 Serum-Free Supplement (Thermo Fisher Scientific #17504) and GlutaMax^{tm}-I supplement (2 mM). Astrocyte differentiation medium contained D-MEM, 1% N2 Supplement (Thermo Fisher Scientific #17502), GlutaMax^{tm}-I supplement (2 mM) and 1% FBS. Oligodendrocyte differentiation medium contained Neurobasal medium, 2% B-27 Serum-Free Supplement (Thermo Fisher Scientific #17504), GlutaMax^{tm}-I supplement (2 mM) and T3 (Sigma #D6397). Cells were fed every 2 days with 2X media for 4 DIV or 10 DIV. At experimental endpoint indicated, cells were fixed with 4% PFA for 15 min at room temperature and immunostained using mouse anti-Tuj1 (neuronal III β-tubulin, 1/500, Covance, Laval, QC, #801202), rat anti-Pdgfrα (1/500, BD PharMingen, #558774) or rat anti-GFAP (1/500, Thermo Fisher Scientific #13-0300). Secondary antibodies were conjugated to Alexa Fluor 568 (as indicated).

Nucleofection

Nucleofection was performed with a Lonza mouse neural stem cell kit according to the manufacturer's instructions (Lonza #VPG-1004). Nucleofections were performed with ~5 million cells dissociated from pooled E12.5 dorsal telencephalons. Nucleofected cells were then seeded for a Neurosphere assay as described except nucleofected cells were cultured for 10 days. To overexpress *Cdkn1a, Cdkn1c* and *Trp73,* cDNAs were cloned into the PiggyBAC Transposon vector (System Biosciences, Inc. #PB530A-2) containing a modified CAG promoter.

TUNEL assay

Cryosections were washed in PBS for 5 min, post-fixed with 4% PFA for 15 min at 37°C, and then permeabilized by Protease K solution provided by a Click-iT Plus TUNEL Assay kit (Invitrogen #C10619). Sections were washed in PBS for 5 min, fixed again in 4% PFA for 5 min at 37°C, rinsed with deionized water and subjected to Click-iT Plus reaction with Alexa Fluor 647 dye using Click-iT Plus TUNEL Assay kit (Invitrogen #C10619) according to the manufacturer's instructions. After Click-iT Plus reaction, brain sections were stained with DAPI (Invitrogen #D1306) and mounted using Aqua-Poly/Mount (Polysciences #18606).

EdU Click it assay

5-ethynyl-2′-deoxyuridine (EdU; Lumiprobe, Cat. 10540) was injected IP at 100 μg/g body weight 24 h before dissection for p-fraction and n-fraction calculations. After cryosection, tissue samples were stained using a Click-iT Plus EdU Imaging Kits (Molecular Probes, Cat. C10640) following the manufacturer's procedures. EdU stained tissue samples were then immunostained with indicated antibodies after 1 h of blocking.

Luciferase Assays

P19 embryonic carcinoma cells (ATCC# CRL-1825) were maintained in Minimum Essential α Medium (GIBCO) supplemented with 10% fetal bovine serum and 50 units/mL penicillin-streptomycin (GIBCO). P19 cells were seeded into 24-well plates (Nalge Nunc) 24 h before transfection. The p*Neurod*^{1kb} (Huang et al., 2000), *Rnd2* (Heng et al., 2008), *Dll1* and *Dll1*-M (Castro et al., 2006) *luciferase* reporters were previously described. Transfections were performed using Lipofectamine 3000 reagent (Invitrogen #L3000015), following the manufacturer's protocol, with 0.5 μg total of expression vector(s) (as indicated in the figure), 0.05 μg firefly luciferase, and 0.025 μg of a Renilla plasmid (transfection control). 24 h post-transfection, transfection media was replaced with fresh media. 24 h later, cells were harvested and firefly luciferase and Renilla activities were measured using the Dual-luciferase Reporter Assay System (Promega #E1910) following the manufacturer's instructions and using a TD 20/20 Luminometer (Turner Designs). Firefly *luciferase* data was normalized by dividing raw light readings by the corresponding Renilla values.

Please cite this article in press as: Han et al., Proneural genes define ground-state rules to regulate neurogenic patterning and cortical folding, Neuron (2021), https://doi.org/10.1016/j.neuron.2021.07.007

Immunoprecipitation (IP)

IPs were performed as described (Han et al., 2018). Briefly, NIH 3T3 (ATCC CRL-1658) cells transfected with pCIG2-*Ascl1* and either pCS108-Flag or pCS108-Flag-*Neurog2* (Han et al., 2018) expression vectors were harvested after 48 h and lysed in NET2 lysis buffer (0.05% NP40, 150 mM NaCl, 50 mM Tris-Cl, pH 7.4) containing protease (1X protease inhibitor complete, 1 mM PMSF), proteasome (7.5 μM MG132) and phosphatase (50 mM NaF, 1 mM $NaOV_3$) inhibitors. 400 μg of protein lysate was immunoprecipitated using anti-FLAG M2 beads (Sigma #A2220) overnight at 4°C. The sample was divided in two and one half was incubated with DNaseI (100 U/mL; Ambion #AM2222). FLAG-beads were washed 5 times in lysis buffer, resuspended in SDS-PAGE loading dye, and run on 8% or 10% SDS-PAGE gels followed by western blot analysis.

Western blot

Western blots were performed as described (Li et al., 2012) with: mouse-anti-Ascl1 (1:10,000, BD Biosciences #556604), rabbit anti-FLAG (1:10,000, Cell signaling #2368), rabbit anti-GAPDH (1:10,000, Cell signaling #2118), rabbit anti-Notch (Cleaved) (NICD, 1:1000, Cell signaling #4147). Western blot signals were converted to a chemiluminescent signal using an ECL kit (EG Healthcare) following the manufacturer's instructions and visualized using X-ray film or a Bio-rad gel doc with GelCapture MicroChemi 2.2.0.0 software.

Proximity Ligation Assay (PLA)

10 um cryo-sections from E12.5 brain were used for the PLA assay. After incubation in blocking solution (10% horse serum in PBST: 1% Triton X-100 in PBS) for 1 h at room temperature, the sections were incubated overnight at room temperature with or without primary antibodies in the blocking solution: rabbit anti-Neurog2 (1:500, Invitrogen #PA5-78556) and mouse anti-Ascl1 (1:100, BD Biosciences #556604). The sections were then washed 3 times in 1X PBST and treated with goat-anti-mouse IgG1 secondary antibodies for 90 min at room temperature. After 3 times washing with 1X PBST, the PLA assay was performed using a Duolink *In Situ* Red Starter Kit Goat/Rabbit (Sigma Aldrich #DUO92105) following the manufacturer's instructions with increased duration of amplification which was overnight in our condition.

RNA-seq

RNA was extracted from cells using MagMAX-96 Total RNA Isolation Kit (Invitrogen, #AM1830) according to the manufacturer's protocol. Strand-specific mRNA sequencing libraries were constructed from 100 ng of total RNA using the TruSeq Stranded mRNA Library Prep Kit (Illumina, San Diego, CA, #20020594) and 125 base paired-end sequence reads were generated on the HiSeq 2500 platform (Illumina). Base calls were generated with RTA v1.18.64 software and pass filter reads were kept for further analysis. Fastq adaptor trimming (Trimmomatic v0.36), quality assessment (FastQC v0.11.6), alignment (STAR v2.5.4a, Samtools v1.9), and transcript quantitation were performed using assembly GRCm38.p6 and Ensembl v94 annotation (Li et al., 2009). Quantitation of aligned reads to transcriptome and gene level summarization were achieved using Kallisto v0.44.0 for transcript isoform read assignment, isoform de-convolution, and quantitation and tximport v1.8.0 for gene level quantitation. Trimmed mean of M values (TMM) normalization was performed using edgeR v3.22.5 (Robinson et al., 2010). We utilized the computational resources of the NIH HPC Biowulf cluster (http://hpc.nih.gov). DESeq2 (Love et al., 2014) was used for identifying differentially expressed genes (DEGs). Heatmaps with Euclidian clustering were generated using Heatmapper (Babicki et al., 2016). GO enrichment analysis was performed by EnrichR (Kuleshov et al., 2016).

Nanostring analysis

Total RNA from FACS sorted cells was isolated with Trizol reagent following the manufacturer's instructions (Life Technologies). RNA integrity and concentration were measured with an Agilent 2100 bioanalyzer. RNA was hybridized to a custom made Nanostring CodeSet (Table S1) and barcodes were counted on an nCounter digital analyzer using the manufacturer's instructions (NanoString Technologies Inc.). Gene expression analyses were performed with nSolver Analysis Software. Gene expression was normalized relative to six spiked positive controls; three reference genes *Actb, Gapdh, Tubb*; and six negative controls to subtract background hybridization.

RT-qPCR

RNA was extracted from cells using Trizol reagent (Thermo Fisher Scientific #15596-026) or RNeasy Micro Kit (QIAGEN, #74004) according to the manufacturer's protocol. cDNA was synthesized with a RT^2 First strand kit (QIAGEN, cat. 330401) and qPCR was performed with RT^2 SYBR Green (QIAGEN, cat. 330500), both using the manufacturer's protocols. Pre-validated RT^2 qPCR primers were from QIAGEN as follows: *Ascl1* (PPM31367F), *Cdkn1a* (PPM02901B), *Cdkn1c* (PPM02895B), *Nestin* (PPM04735A), *NeuN* (PPM60749A), *Neurog2* (PPM28944A), *Pax6* (PPM04498B), *Tbr2* (PPM32970F), and *Trp73* (PPM03436B). Three reference genes were used in each assay: *Gapdh* (PPM02946E), *B2m* (PPM03562A) and *Hprt* (PPM03559F). qPCR was performed with three biological replicates (N; RNA from three embryos) and three technical replicates per sample (n). Relative gene expression was determined using the delta-delta Cq method standardizing relative to reference genes (*Gapdh, B2m, Hprt)* and normalizing to pro^- NPC values (set at 1).

ATAC-seq

$CD15^+$ GFP/mCherry negative, single, double positive cortical NPCs were dissociated from E12.5 $Neurog2^{Flag\text{-}mCherryKI/+}$;$Ascl1^{GFPKI/+}$ cortical tissue. ATAC-seq was performed as previously described, using 50,000 cells as input material for the transposase reaction with

Please cite this article in press as: Han et al., Proneural genes define ground-state rules to regulate neurogenic patterning and cortical folding, Neuron (2021), https://doi.org/10.1016/j.neuron.2021.07.007

Nextera DNA library preparation Kit (Cat. No. FC-121-1030) (Buenrostro et al., 2015). Sequencing was performed with three biological replicates to a depth of approximately ~330 million reads to delineate TF footprints. Reads were aligned on the reference genome GRCm38 using Burrows-Wheeler Aligner 0.7.12 (BWA) (Li and Durbin, 2009) with initial quality control using FastQC . Heatmaps and average plots for the ATAC-seq reads near TSS were generated by NGSPLOT tool (Shen et al., 2014) after merging the replicates of samples into a single BAM file and eliminating the duplications of reads. To identify bona fide open regulatory regions (i.e., true regions of local enrichment relative to the background ATAC-seq signal), we employed a commonly used hotspot (HS) algorithm with a FDR < 0.01 (John et al., 2011). We further refined our analysis by only examining HSs present in all three biological replicates, yielding one high confidence dataset. Differentially accessible sites (DASs) were identified using statistical routines implemented in the DiffBind Bioconductor package (Ross-Innes et al., 2012). A merging function was used to find all overlapping HSs and to derive a single unique set of intervals for all samples to apply normalization and statistical testing using an edgeR Bioconductor package. Each consensus interval in the Diffbind analysis was annotated and the distance to the nearest promoter and corresponding gene id was added using the ChIPpeakAnno package. To predict which TF was binding to the unique regulatory regions in each cell type, we first used the Wellington algorithm to identify TF footprints within the ATAC-seq peaks (Piper et al., 2013), and then used the Homer annotate peaks tool to identify known TF motifs (Heinz et al., 2010).

ChIP seq

Ascl1 ChIP from embryonic telencephalon was performed as previously described (Castro et al., 2006). Libraries were prepared using NEBNext Ultra II DNA library prep kit from Illumina without size-selection and following the manufacturer's instructions, and sequenced using NEXT Seq 500 at the Instituto Gulbenkian de Ciência genomic facility. Raw reads were mapped using Bowtie version 0.12.7 and peak calling performed using MACS version 2.1.1 using default settings. The peaks from Neurog2 and Ascl1 ChIP-seq data were assigned to nearest TSSs obtained from (ftp://ccg.vital-it.ch/epdnew/M_musculus/003/db/promoter_ucsc.txt). Then, the TSSs bound by both Neurog2 and Ascl1 (i.e., peaks are overlapping) were visualized by Integrative Genomics Viewer version (IGV) 2.8.2.

Gene regulation network analysis (GRN) and *in silico* perturbation assay

GRN analysis was performed using the program codes from (Okawa et al., 2015). Briefly, GRNs for pro$^-$, Neurog2$^+$, Ascl1$^+$ and double$^+$ NPCs were built using population specific TFs that were differentially expressed in each population with respect to the proneural neg population. GRN for proneural negative NPCs was built using the union of differentially expressed TFs against the other three NPCs. Neurog2 and Ascl1 targets were identified using E14.5 telencephalic Neurog2 ChIP-seq data (Sessa et al., 2017) and Ascl1 (this study) ChIP-seq data. Transcriptional interactions were obtained as the union of the two ChIP-seq data and the MetaCore database. Interactions were removed if the chromatin regions of target genes were not open in all ATAC-seq replicates. After building GRNs, *in silico* perturbation assays were performed by repressing the expression of either Neurog2 or Ascl1, or both together. The GRN simulation was carried out by the Boolean network formalism using the inhibitor dominant logic rule. When GRN reached a steady state, repressed genes were identified. Cytoscape was used for visualization of GRNs (Shannon et al., 2003).

scRNA-seq data analysis of human COs and fetal cortices

scRNA-seq data of human COs was obtained from GSE137877 (Sivitilli et al., 2020). Further processing and analyses were performed with the Seurat v.3.2.3 R package (Butler et al., 2018). Cells that were of low quality or represented doublets were excluded by filtering out cells with greater than 4000 and fewer than 500 genes. The data was then transformed by the SCTransform function while regressing out the variance due to mitochondrial RNAs. Clustering was performed by the RuNPCA, FindNeighbors and FindClusters functions using the first 30 principal components. The 2D projection of the clustering was carried out by the RunUMAP function. The annotation of cell type to each cluster was performed by using the same set of markers as in (Sivitilli et al., 2020). The numbers of pro$^-$, Neurog2$^+$, Ascl1$^+$ and double$^+$ cells were counted with the expression threshold > 0. A pseudotime analysis was performed on week 12 cells expressing Neurog2 and/or Ascl1 with or without DLX1/2$^+$ population using the Monocle3 R package (Qiu et al., 2017). The input genes were DEGs determined by the differential GeneTest function with the adjusted p value cutoff < 0.001. The scRNA-seq data of human fetal cortex was obtained from GSE104276 (Zhong et al., 2018). The numbers of pro$^-$, Neurog2$^+$, Ascl1$^+$ and double$^+$ cells were counted among the NPCs in each gestation week.

Droplet digital PCR

A QX200 droplet digital PCR (ddPCR) system (Bio-Rad) was used to quantify recombination efficiency of the *RC::L-DTA* locus in *split-Cre* mice. The recombined *DTA* locus flips its orientation so that the *DTA* transgene is in its correct orientation downstream of the CAG promoter. We detected this recombined allele using a forward primer 5′-GGT TAT TGT GCT GTC TCA TCA TTT-3′, reverse primer 5′-AGA AGA ATC AAC AAC ATC ATC AGC-3′, and probe 5′-6-FAM-TAC TAG TCA-ZEN-ATT GGC CAC CAT GGG C-Iowa Black FQ-3′ (Integrated DNA Technologies, Coralville, IA, USA) sequences. The *ApoB* forward primer 5′-CGT GGG CTC CAG CAT TCT A-3′, reverse primer 5′-TCA CCA GTC ATT TCT GCC TT TG-3′, and probe 5′-HEX-CCT TGA GCA-ZEN-GTG CCC GAC CAT TC- Iowa Black FQ-3′ (Integrated DNA Technologies) sequences were used for normalization of *DTA* gene copies per cell. The ddPCR reaction was performed in a 20 μL volume containing 10 μL of 2X QX200 ddPCR Supermix for Probes (No dUP) (Catalog# 1863023, Bio-Rad), 10 ng of genomic DNA, 900 nM of the forward and reverse DTA primers, 250 nM of *DTA* probes (this study, Table

Please cite this article in press as: Han et al., Proneural genes define ground-state rules to regulate neurogenic patterning and cortical folding, Neuron (2021), https://doi.org/10.1016/j.neuron.2021.07.007

S6), 900 nM of the forward and reverse *ApoB* primers, and 250 nM of the *ApoB* probe (Weber-Adrian et al., 2021). Each ddPCR assay mixture was loaded into a disposable droplet generator cartridge (Catalog# 1864008, Bio-Rad). Then, 70 μL of droplet generation oil for probes (Catalog# 1863005, Bio-Rad) was loaded into each of the eight oil wells. The cartridge was then placed inside the QX200 droplet generator (Bio-Rad). When droplet generation was completed, the droplets were transferred to a ddPCR 96-well plate (Catalog# 12001925, Bio-Rad) using a multichannel pipet. The plate was heat-sealed with foil and placed in C1000 Touch Thermal Cycler (Bio-Rad). Thermal cycling conditions were as follows: 95°C for 10 min, then 50 cycles of 94°C for 30 s and 60°C for 2 min, and 98°C for 10 min, and a 4°C indefinite hold. FAM fluorescent signal for *DTA* DNA sequence and HEX fluorescent signal for *ApoB* gene sequence in each droplet were counted using a QX200 digital droplet reader, and analyzed by QuantaSoft analysis software ver.1.7.4.0917 (Bio-Rad). All ddPCR analyses were performed at the Sunnybrook Research Institute Genomics Core Facility.

QUANTIFICATION AND STATISTICAL ANALYSIS

All experiments used for statistical analysis were performed a minimum of three times (biological repeats from individual embryos and independent experiments, represented by N-values, as indicated in the figure legends. Individual biological replicates (N) are shown as individual dots in the plots after averaging technical replicates. All statistical analysis was performed using GraphPad Prism Software version 8.0 (GraphPad Software). Unpaired two tailed Student's t tests were used to calculate statistical significance between two experimental groups. For multiple comparison between more than two experimental groups, one-way ANOVAs with Tukey post hoc analyses were used. Error bars represent standard error of the mean (SEM). p values: ns - not significant, < 0.05 *, < 0.01 **, < 0.001 ***. Significance was defined as p values less than 0.05.

Imaging and image processing methods

Images of stained sections and cells were obtained using a Leica DMI8 fluorescent microscope or a Zeiss Axiovert 200M confocal microscope. Immunolabeled cells or RNAscope signals (with > 1 mRNA puncta/cell) were counted using manual counting, CellProfiler (McQuin et al., 2018) and Fiji (ImageJ) software (Schindelin et al., 2012). All data points shown in the graphs are the average values of the sequential sections in individual biological replicates. Representative regions of interest (ROI) are presented in the figures and were used for counting or analyzing. To define the individual cells that have positive signals in immunostained images, binary data was generated by applying combinations of cell segmentation with Find Maxima and auto threshold functions using Otsu or Li algorithms. The binary images corresponding to individual cells were then counted by applying the average cell size and circularities. For counting co-expressed cells, the "AND" function of image calculator in Fiji (ImageJ) was applied to make binary images of two channels above the threshold and by counting output binary data having dual stained cells. A different strategy was used for counting BrdU and EdU stained cells due to puncta shapes in the nucleus. First, the DAPI image was used to define the nucleus of individual cells. Then, nuclei with more than 50% coverage by BrdU or EdU signals were counted as above the threshold. Next, BdU and EdU positive nuclei were subjected for counting co-expression of the other markers using the same strategy as described above. Line plots and 3D surface plots for RNAscope signals were generated by the Plot Profile and 3D Surface Plot functions of Fiji (ImageJ) software. Distance map analysis for *Hes1* and *Dll1* RNAscope signals were performed using the Geometry to Distance Map function with 150 threshold and inverse options of Fiji (ImageJ) software. The mean value from Geometry to Distance Map analysis was calculated and compared between the groups.

Identification of VZ and non VZ

We identified zonal boundaries in the embryonic cortex using DAPI images. The VZ was distinguished by well-aligned nuclei perpendicular to the ventricular surface, and the SVZ by random nuclear orientations. After making the boundary between VZ and SVZ, we set an ROI for VZ and non VZ for automatic counting and quantified markers using Fiji (ImageJ) software. White dashed lines in figures are boundaries that we used for VZ and SVZ separation.

Calculation of local gyrification index (GI)

Images of P0 control and *split-Cre;deleter* cortices were used to calculate local GI values using a modified version of a published protocol (Matsumoto et al., 2017). Briefly, Satb2 immunostaining was used to identify the superior limits of the upper cortical layers. We then placed two spots ~500 um apart to cover the imaged sections. Then, two lines were drawn between two spots to measure two lengths: (A) the length of a direct line between the two spots, (B) the actual length between two spots on upper layer surface defined by tracing the upper limit of Satb2 staining. After measuring (A) and (B), local GI value was calculated by the below equation.

$$\textit{Local gyrification index } (GI) = \frac{(B)\ \textit{actual length between two spots on upper layer surface}}{(A)\ \textit{length from direct line between two spots}}$$

The average value of the calculated local GI from each animal were applied for statistical comparisons and presented in the figure.

Curvature analysis of radial glia (RG) trajectories

100 μm vibratome sections from E18.5/P0 brains of control and *split-Cre;RC::L-DTA* were immunostained with BLBP antibodies to label RG fibers. From BLBP stained images, individual RG fibers were carefully traced to generate the images having traced RG fibers

Please cite this article in press as: Han et al., Proneural genes define ground-state rules to regulate neurogenic patterning and cortical folding, Neuron (2021), https://doi.org/10.1016/j.neuron.2021.07.007

with green or orange color on black backgrounds (Figure 6P). The traced RG fibers were then subjected to analyzing curvature indices using Fiji (ImageJ) plugin, Kappa ver. 1.7.3 with a Squared Distance Minimization data fitting algorithm to calculate average curvature indices of each RG fiber.

Analysis of Variance Indices

To compare *NEUROG2, ASCL1* and *HES1* transcript distribution to control transcripts (*PAX6, HOPX, POLR2A, PPIB, UBC*), we calculated a variance index as a measure of irregularity. Boxes were drawn to encompass area 17 of the macaque visual cortex (lateral – X:3000 um, Y:1200 um and medial – X:2500 um, Y: 1000 um). VZ to oSVZ areas were extracted to analyze RNAscope intensity signals using the Plot profile function in Fiji (ImageJ). RNAscope intensities were then normalized to DAPI intensity. The calculated relative fluorescence intensities (relative F.I) were plotted on a line plot and used to calculate a variance index. Briefly, expression levels for each line plot were standardized to have an overall mean value = 1, by normalizing to the mean relative FI. For each gene, we extracted data from 0-2500 um of the x axis. We calculate the standard deviation from the standardized data as a "variation index." Controls pooled data from five genes (*PAX6, HOPX, POLR2A, PPIB, UBC*). Two-tailed Student t tests were used to individually compare variance indices of control genes to *NEUROG2, ASCL1* and *HES1*.